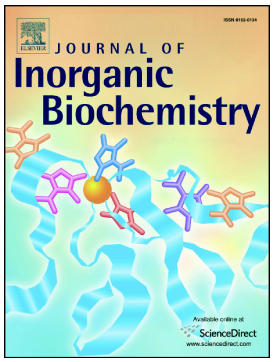

Synthesis, chemical characterization, PARP inhibition, DNA binding and cellular uptake of novel ruthenium(II)-arene complexes bearing benzamide derivatives in human breast cancer cells

Marijana Pavlović, Ana Tadić, Nevenka Gligorijević, Jelena Poljarević, Tamara Petrović, Biljana Dojčinović, Aleksandar Savić, Siniša Radulović, Sanja Grgurić-Šipka, Sandra Aranđelović

PII: S0162-0134(20)30183-5

DOI: https://doi.org/10.1016/j.jinorgbio.2020.111155

Reference: JIB 111155

To appear in: *Journal of Inorganic Biochemistry*

Received date: 7 April 2020

Revised date: 3 June 2020

Accepted date: 11 June 2020

Please cite this article as: M. Pavlović, A. Tadić, N. Gligorijević, et al., Synthesis, chemical characterization, PARP inhibition, DNA binding and cellular uptake of novel ruthenium(II)-arene complexes bearing benzamide derivatives in human breast cancer cells, *Journal of Inorganic Biochemistry* (2020), https://doi.org/10.1016/j.jinorgbio.2020.111155

Synthesis, Chemical characterization, PARP Inhibition, DNA Binding and Cellular Uptake of Novel Ruthenium(II)-Arene Complexes Bearing Benzamide Derivatives in Human Breast Cancer Cells

Marijana Pavlović,[a] Ana Tadić,[b] Nevenka Gligorijević,[a] Jelena Poljarević,[b] Tamara Petrović,[b] Biljana Dojčinović,[c] Aleksandar Savić,[b] Siniša Radulović,[a] Sanja Grgurić-Šipka,[b*] Sandra Aranđelović[a]

[a]Department of Experimental Oncology Institute for Oncology and Radiology of Serbia Pasterova 14, 11000 Belgrade, Serbia

[b]Department of General and Inorganic Chemistry Faculty of Chemistry, University of Belgrade Studentski trg 12-16, 11000 Belgrade, Serbia

[c]Centre of Chemistry Institute of Chemistry, Technology and Metallurgy, University of Belgrade Studentski trg 12-16, 11000 Belgrade, Serbia

*corresponding authors: Sanja Grgurić-Šipka, sanjag@chem.bg.ac.rs, +381113336736; Jelena Poljarević, jelenal@chem.bg.ac.rs, +381113336736

Abstract

Inhibitors of poly(ADP-ribose) polymerase-1 (PARP-1) showed remarkable clinical efficacy in *BRCA*-mutated tumors. Based on the rational drug design, derivatives of PARP inhibitor 3-aminobenzamide (3-AB), 2-amino-4-methylbenzamide (**L1**) and 3-amino-N-methylbenzamide (**L2**), were coordinated to the ruthenium(II) ion, to form potential drugs affecting DNA and inhibiting PARP enzyme. The four conjugated complexes of formula: **C1** [(η^6-toluene)Ru(**L1)**Cl]PF_6, **C2** [(η^6-*p*-cymene)Ru(**L1)**Cl]PF_6, **C3** [(η^6-toluene)Ru(**L2)**Cl_2] and **C4** [(η^6-*p*-cymene)Ru(**L2)**Cl_2], have been synthesized and characterized. MTT assay showed the highest antiproliferative activity of **C1** in HCC1937, MDA-MB-231, and MCF-7 breast cancer cells. Efficiency of inhibition of PARP-1 enzymatic activity *in vitro* decreased in order: **C2**>**C4**>3-AB>**C1**>**C3**. ICP-MS study of intracellular accumulation and

distribution in *BRCA1*-mutated HCC1937 revealed that **C1-C4** entered cells within 24 h. The complex **C1** showed the highest intracellular accumulation, nuclear-targeting properties, and exhibited the highest DNA binding (39.2±0.6 pg of Ru per μg of DNA) that resulted in the cell cycle arrest in the S phase.

Keywords: antitumor agents; breast cancer; PARP inhibitor; ruthenium(II)

1. Introduction

Rapid increase in the number of cancer deaths worldwide makes drug development research highly important. Nowadays, it is well known that novel antitumor drugs developed to replace cisplatin need to outweigh severe adverse effects and accompanying resistance induced by cisplatin [1-3]. Ruthenium-based compounds are one of the most promising metal-based anticancer drug candidates [4]. The synthetic chemistry of ruthenium complexes is very well established and gives access to a large variety of compounds [5]. Among all synthesized ruthenium complexes so far, ruthenium(III) complexes, NAMI-A (imidazolium-*trans*-[tetrachloro-(dimethylsulfoxide)imidazole ruthenium(III)]), which acts on metastases of solid tumors [6], and KP1339 (sodium-*trans*-[tetrachlorobis(1H-indazole)ruthenium(III)]), which is effective against platinum-resistant tumors [7], completed phase II clinical trials [8-13]. Organometallic ruthenium(II)-arene compounds with completely different metallodrug scaffold, in which three of the coordination sites are occupied by η^6-coordinated arene that stabilizes Ru^{+2} oxidation state, are being under intensive development [14]. RAPTA-C ([Ru(η^6-*p*-cymene)(pta)Cl_2], pta=1,3,5-triaza-7-phosphatricyclo[3.3.1.1]decane), RAED-C ([Ru(η^6-*p*-cymene)(en)Cl][PF_6], en=ethylenediamine), and RAPTA-T ([Ru(η^6-toluene)(pta)Cl_2]), showed to be effective in reducing the number and weight of lung metastases [15-19]. To date, a myriad of structurally different ruthenium(II)-arene complexes have been prepared, with some of them exhibiting notable anticancer activities *in vitro* [20-26]. Ruthenium(II) have similar ligand exchange kinetics to platinum(II), and the octahedral

geometry of ruthenium complexes offers unique possibilities for binding to nucleic acids [27-28].

The numerous still ongoing studies of mechanisms of action of cisplatin and ruthenium-based drugs emphasize the existence of more variable cellular targets of these agents beyond nuclear DNA [29-32]. The particular interest is in investigating enzyme inhibition by metal complexes [33]. In that aspect, Kilpin and Dyson proposed the classification of metal-based enzyme inhibitors to several groups [34], depending on whether the activity of metal complexes relies mostly on the chemical properties of metal centre, bioactive ligand, or was influenced by the combination of both.

Particularly interesting family of enzymes present in eukaryotes are poly(ADP-ribose) polymerases (PARPs), which are involved in various cellular processes, including DNA repair, chromatin remodeling, transcriptional regulation, and cell death [35-37]. PARP-1 is one of the most abundant chromatin-bound protein, accounting for >90% of total PARP activity [38]. It is considered to be a key player in DNA base excision repair (BER) and repair of single-strand DNA breaks (SSBs) in response to ionizing radiation, oxidative stress, or DNA-binding agents [39-40]. Structurally, PARP-1 is comprised of three distinct functional domains: (1) N-terminal DNA-binding domain containing three zinc fingers important for the PARP-1 binding to DNA breaks, (2) central automodification domain serving as an acceptor of ADP-ribose moieties, and (3) C-terminal catalytic domain forming active site of PARP-1 ("PARP signature") that transfers ADP-ribose subunits from NAD^+ to protein acceptors (Figure 1) [41,42].

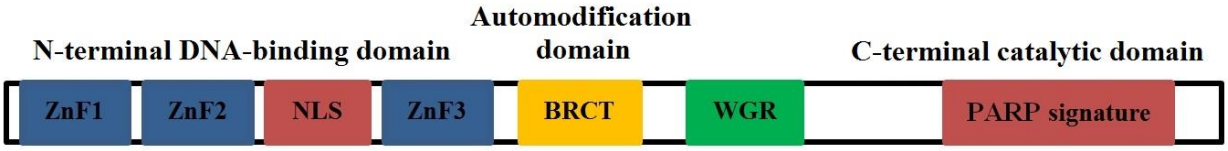

Figure 1. Structural and functional organization of human PARP-1 enzyme. ZnF1, ZnF2 and ZnF3, zinc fingers 1, 2 and 3; NLS, nuclear localization signal; BRCT, BRCA1 C-terminus; WGR, domain formed of tryptophan (W), glycine (G) and arginine (R) amino acids.

PARP-1 utilizes beta nicotinamide adenine dinucleotide (β-NAD^+) as a substrate to covalently add poly(ADP-ribose) (PAR) chains onto itself and other nuclear acceptor proteins, in a process termed PARylation [43]. The role of PARP-1in DNA damage response and cell death regulation prompted the development of potent small molecules named PARP inhibitors (PARPi) [39]. Generally, PARPi are designated as competitive inhibitors, since they impair the catalytic activity of PARP-1 by interacting with the NAD^+ binding site [44]. Nicotinamide, benzamide, and 3-aminobenzamide (3-AB) were identified as the first generation of "classical" PARPi [45]. Despite the limited potency and specificity to be used in clinics, these compounds are significant for research purposes [46]. Structure-activity relationship analysis showed that potent PARPi should have an electron-rich aromatic or polyaromatic heterocyclic system, bearing a pharmacophore with *cis*-configurated carboxamide, imide, or a carbamoyl group [47]. To date, four PARPi of the third generation (olaparib, rucaparib, niraparib, and talazoparib) were approved by the United States Food and Drug Administration (U.S. FDA) (Figure 2) [42, 48-50], as single-agent therapy, for targeting breast cancer susceptibility genes (*BRCA*)-mutated breast, ovarian, prostate, and pancreatic cancers [51]. PARPi are the first clinically approved drugs designed to exploit synthetic lethality concept in tumors harboring mutations in *BRCA1* or *BRCA2* genes, responsible for the repair of double-strand DNA breaks (DSBs) by homologous recombination (HR) [52,53]. Synthetic lethality is a genetic concept based on the idea that defect in either one of two genes has little effect on the cell or organism, but a combination of defects in both genes results in cell death [54]. The cells with impaired HR pathway are dependent on alternative ways for DNA repair and survival, and thereby PARPi became promising therapy for *BRCA*-mutated cancers.

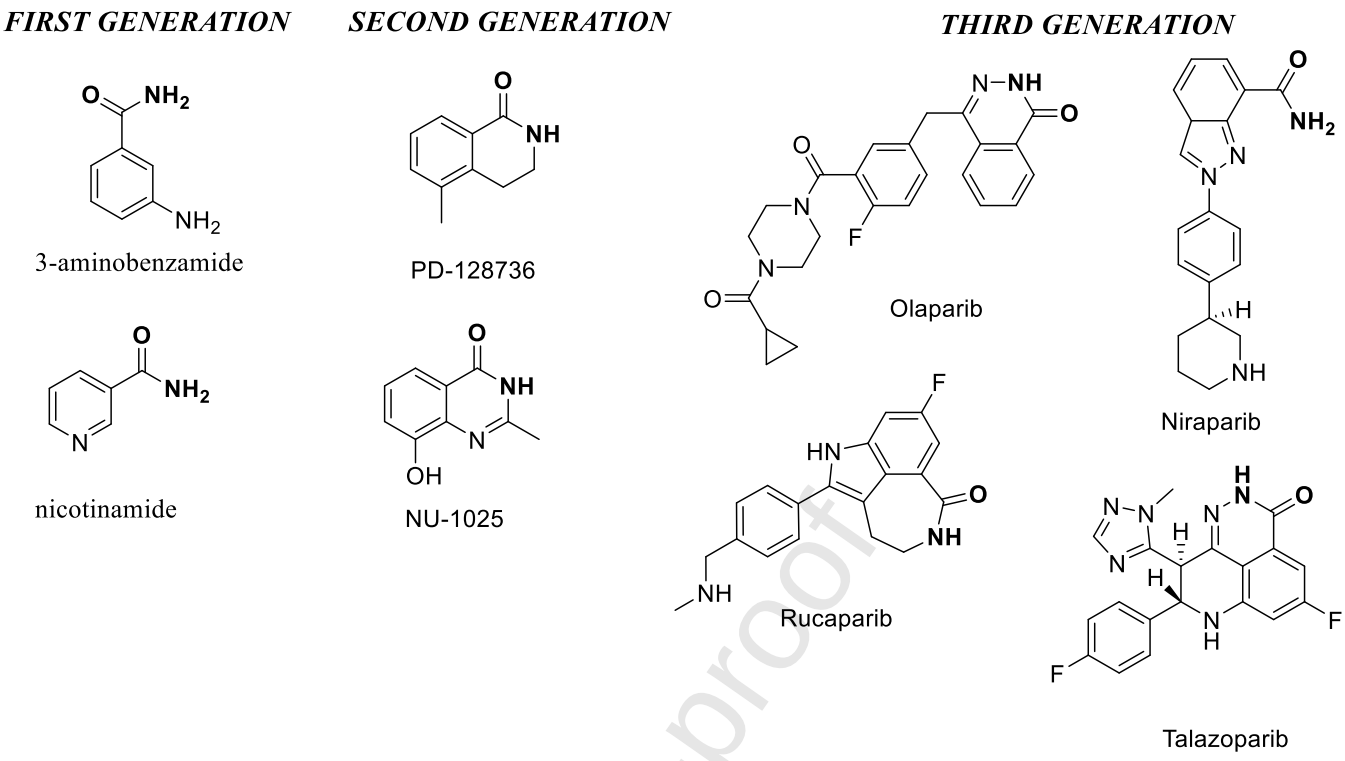

Figure 2. Structure of various PARP inhibitors. Bold is the common amide moiety in all PARP inhibitors

Although recent reports suggested that the application of PARPi could be extended to "BRCAness" tumors with defects in HR repair genes other than *BRCA1* and *BRCA2* [55-57], the acquired resistance caused by arising secondary mutations in HR repair genes that restore the function of HR repair pathway limits the clinical efficacy of PARPi as single agents [58]. Therefore, combination therapy is a reasonable approach to improve the utility of these inhibitors to serve as chemopotentiators of commonly used cytotoxic chemotherapeutics, such as cisplatin [59-62]. Unfortunately, multicomponent drug cocktails can display adverse effects caused by complex pharmacokinetics and unpredictable drug-drug interactions. Hence, multi-targeting single drugs offer some advantages of pharmacokinetic simplicity and improved outcomes [35].

Growing tendency in the drug design area is to connect metals with pharmacophoric moieties of bioactive ligand, to achieve different spectra of biological activity and improve the properties of both constituents [29,32,63,64]. Reports up to date showed that different ruthenium(II)-arene complexes entered tumor cells efficiently and bound DNA [24,65].

Therefore, they may present appropriate scaffold to bring bioactive ligands with PARP-1 inhibitory potential more closely to their targets in the cell. Additionally, the study performed by Mendes *et al* has shown that compounds based on platinum, ruthenium, or gold may display high PARP-1 inhibitory activity, supporting the model whereby displacement of zink from the zinkfinger motif of PARP-1 by metal ions led to decreased PARP-1 activity [66].

In the present study, novel ruthenium(II)-arene complexes carrying 3-AB derivatives as ligands, were synthesized and examined for the inhibitory potential against the catalytic activity of PARP-1. Further, their growth inhibitory effects were investigated in a panel of human breast cancer cell lines, which were either *BRCA1*-mutant, triple-negative, or hormone-responsive. To reveal the mechanism of action and intracellular targets, we analyzed cell cycle progression, binding to DNA, cellular uptake, and distribution across cellular compartments of treated cells. The influence of the particular structural changes in the molecules on the different aspects of anticancer potential is discussed.

2. Experimental Section

2.1. Material and Methods

$RuCl_3 \cdot 3H_2O$ was purchased from Johnson Matthey (London, UK). 2-amino-4-methylbenzamide (**L1**) and 3-amino-N-methylbenzamide (**L2**) were purchased from Sigma Aldrich. $[Ru(\eta^6\text{-}p\text{-cymene})Cl_2]_2$ was prepared according to a published procedure [67]. $[Ru(\eta^6\text{-toluene})Cl_2]_2$ was prepared according to a published procedure [68]. Solvents were obtained and used without further purification. Infrared spectra were recorded on Nicolet 6700 FTIR spectrometer, using the ATR technique. ^1H and ^{13}C spectra were recorded on Bruker Avance III 500 spectrometer. Chemical shifts for ^1H and ^{13}C were referenced to residual ^1H and ^{13}C present in d_6-DMSO and d_4-CD_3OD. Conductivity measurements were done using a CrisonMultimeter MM 41 instrument. Conductivities of complexes were obtained with 1mM solutions in dimethyl sulfoxide (DMSO). ESI mass spectra were measured on a mass spectrometer (Bruker, Model Esquire 3000), using CH_3CN/CH_3OH as a

solvent. Elemental analyses were performed at the Microanalytical Service of the Faculty of Chemistry of the University of Vienna.

NMR spectra of all synthesized compounds are given in Supplementary materials Figure **S1 – S10.**

2.2. Synthesis of Complexes

Synthesis of [(η^6-toluene)Ru(L1)Cl]PF_6 (C1). A suspension of **L1** (0.028 g, 0.190 mmol) in methanol (3 mL) was added to suspension of (0.050 g, 0.095 mmol) [Ru(η^6-toluene)Cl_2]$_2$ in methanol (3 mL). The reaction mixture was stirred at room temperature for 1h. The yellow solution was concentrated in vacuo (to 2 mL) and solid NH_4PF_6 (0.03 g) was added. The mixture was stirred at room temperature for 2h. The resultant yellow precipitate was filtered off and dried in vacuo. Yield 55%.

IR (ATR) ν_{max}/cm^{-1}: 844.1 - 666.3 (ar**C-H** δ oop), 1436.9 (N-CO stval) 1534 (N-CO stsym), 1592 (N-H δ, NH_2 amide and amine), 1646 (**C=O** st), 3126.0 (ar**C-H** st), 3253.7 – 3309.9 (**NH_2**st)

^{1}H NMR (500 MHz, [D_6]DMSO δ(ppm) (Figure S1): 2,14 and 2.20 (s, 3H, C**H_3**(toluene)); 2,16 (s, 3H, C**H_3**(L1)); 5.70 – 6.16 (4H, C2 – C6 toluene); 6.31 (m, 1H, C3(L1)) and 6.47 (s, 1H, C5(L1))6.60(m, 2H, N**H_2** (L1)); 6.93 and 7.60 (s, 2H, N**H_2**=CO- (L1)); 7.41-7.43 (d, 1H, C6 (L1)).

^{13}C NMR (50 MHz, [D_6]DMSO δ(ppm) (Figure S2): 18.54 (-**C**H_3, toluene); 21.06 (-**C**H_3, L1); 82.19; 84.30; 89.45, 93.02, 96.45, 105.38 (6C, (**C**H(toluene)); 111.16; 115.70; 116.50; 128.79; 141.61 and 150.25 (6C, **C**H(L1)) i 171.21 (**C**=O).

ESI/MS (m/z): negative mode 377 [M–PF_6-H]$^-$ (calc. for $RuC_{15}H_{17}N_2OCl$ 377.6)and 413 [M–PF_6+Cl]$^-$ (calc. for $RuC_{15}H_{17}N_2OCl_2$413,1); positive mode 343 [M–PF_6-Cl]$^+$ (calc. for $RuC_{15}H_{17}N_2O$ 343,1)

Elemental analysis: calc. for $RuC_{15}H_{18}N_2OClPF_6 \cdot H_2O$ (%) C, 33.23; H, 3.69; N, 5.17; found (%): C, 33.21; H, 3.60; N, 5.60.

Synthesis of [(η^6-*p*-cymene)Ru(L1)Cl]PF_6 (C2). A suspension of **L1** (0.0245 g, 0.164 mmol) in methanol (3 mL) was added to suspension of [Ru(η^6-*p*-cymene)Cl_2]$_2$ (0.0500 g, 0.082 mmol) in methanol (3 mL) and left stirring at room temperature. After 24h, solid NH_4PF_6 (0.05g) was added into this yellow solution. The reaction mixture was concentrated in vacuo (to 2 mL) and diethyl ether was added. The yellow precipitate was filtered off and dried in vacuo. Yield 63.9%.

IR (ATR) ν_{max}/cm^{-1}: 837.8 (ar**C-H** δ oop), 1408.7 (N-CO stval) 1549.6 (N-CO st sym), 1565 (N-H δ, NH_2 amide and amine), 1647.9 (**C=O** st), 2973.0 – 3213.3 (ar**C-H** st), 3310.7 and 3455.2 (**NH_2** st amide and amine N-H)

^{1}H NMR (500 MHz, [D_4]CD_3OD δ(ppm) (Figure S4): 1.19 – 1.24 (m, 6H, (C**H_3**)$_2$CH (cymene)); 1.90 (s, 3H, C**H_3** (cymene)); 2.50 (s, 3H, CH_3 (L1)); 2.60 (m, 1H, $(CH_3)_2$C**H** (cymene)); 5.30 – 5.29 (d, 1H, C**2**(cymene)); 5.39 – 5.45(dd, 2H, C3,5, cymene); 5.58 – 5.57 (d, 1H, C2(cymene)); 7.22 – 7.23 (d, 1H, C3(L1)); 7.47 (d, 1H, C5 (L1)); 7.65 – 7.66 (d, 1H, C6(L1)).

^{13}C NMR (50 MHz, [D_4]CD_3OD δ(ppm) (Figure S5): 17.86 (-**C**H_3(cymene)); 22.03 and 22.55 (2C, -CH(**C**H_3)$_2$); 32.09 (**C**H3, L1); 79.50, 81.94, 82.98, 82.94 and 96.15 (6C, (**C**H(cymene)); 101.8, 122.78, 127.70, 133.08, 143.23 and146.97 (6C, **C**H(L1)); 174.12 (**C**=O (L1)).

^{1}H NMR (500 MHz, [D_6]DMSO δ(ppm) 1.18 – 1.20 (m, 6H, (C**H_3**)$_2$CH (cymene)); 2.09 (s, 3H, C**H_3** (cymene)); 2.14 (s, 3H, CH_3 (C2-L1)); 2.83 (m, 1H, $(CH_3)_2$C**H** (cymene)); 5.73 – 5.80 (d, 4H, C2, C3, C5, C6(cymene)); 6.30-6.29 (d, 1H, C3(L1)); 6.47 (d, 1H, C5(L1));6.52(m, 2H, N**H**$_2$ (C2-L1)); 7.61 and 6.92 (s, 2H, N**H_2**=CO- (L1)); 7.44 – 7.42 (d, 1H, C6(L1)).

^{13}C NMR (50 MHz, [D_6]DMSO δ(ppm)): 17.73 (-**C**H_3(cymene)); 21.48 (2C, -CH(**C**H_3)$_2$); 30.33 (**C**H3, L1); 85.67, 85.42, 99, 97 and 106.21 (6C, (**C**H(cymene)); 111.52, 115.75, 128.78, 141.30 (6C, **C**H(L1)); 171.37 (**C**=O (L1)).

ESI/MS (m/z): negative mode 419 $[M–PF_6\text{-}H]^-$ (calc. for $RuC_{18}H_{23}N_2OCl$ 419.6) and 455 $[M–PF_6+Cl]^-$ ($RuC_{18}H_{23}N_2OCl_2$ 455.1); positive mode 385 $[M–PF_6\text{-}Cl]^+$ (calc. for $RuC_{18}H_{23}N_2O$ 385.6)

Elemental analysis: calc. for $RuC_{18}H_{24}N_2OClPF_6$(%) C, 38.19; H, 4.24; N, 4.95; found (%): C, 38.58; H, 3.89; N, 5.18.

Synthesis of [(η^6-toluene)Ru(L2)Cl_2] (C3). Solid **L2** (0.028 g, 0.190 mmol) and [Ru(η^6-toluene)Cl_2]$_2$ (0.0500 g, 0.095 mmol)) were suspended in 20 mL of methanol and left to stir at room temperature for 24h. The orange precipitate was filtered off and dried in vacuo. Yield 40%.

IR (ATR) ν_{max}/cm^{-1}: 856-695 (ar**C-H** δ oop), 1544 (N-CO st sym, **NH_2** δ), 1592 (N-H δ, NH_2 amide and amine), 1634 (**C=O**st), 3028 (ar**C-H**st), 3317-3137 (**NH_2**st and **NH**val)

^{1}H NMR (500 MHz, [D_6]DMSO δ(ppm) (Figure S7): 2.02 (s, 3H, C**H_3**(toluene)); 2.61 (d, 3H, -NH-C**H_3**); 5.22 (s, 2H, -N**H_2**); 5.59 i 5.87 (m, t, 5H, C**H**(toluene)); 6.54; 6.79; 6.89 and 6.93(dd, dd, t, t, 4H, C**H**(arene)) and 8.04 (d, 1H, N**H**).

^{13}C NMR (50 MHz, [D_6]DMSO δ(ppm) (Figure S8): 20.54 (-**C**H_3); 28.20 (-NH-**C**H_3); 84.20; 86.81; 91.46 and107.59 (6C, (**C**H(toluene)); 114.77; 116.08; 118.24; 130.60; 137.51 and 150.66 (6C, **C**H(arene)); 169,40 (**C**=O)

ESI/MS (m/z): negative mode 451 $[M+Cl]^-$ (calc. for $RuC_{15}H_{18}N_2OCl_3$449.6) and413$[M\text{-}H]^-$ (calc. for $RuC_{15}H_{17}N_2OCl_2$ 413.1); positive mode 343 $[M–2Cl]^+$ (calc. for $RuC_{15}H_{17}N_2O$ 343.1)

Elemental analysis: calc. for $RuC_{15}H_{18}N_2OCl_2$(%) C, 43.47; H, 4.35; N, 6.76; found (%): C, 43.19; H, 4.51; N, 6.75.

Synthesis of [(η^6-*p*-cymene)Ru(L2)Cl_2] (C4). A suspension of [Ru(η^6-*p*-cymene)Cl_2]$_2$ (0.0500 g, 0.082 mmol) and **L2** (0.0245 g, 0.164mmol) in 10 mL of methanol was left stirred under Ar atmosphere at room temperature for 48 h. The orange precipitate was filtered off and dried in vacuo. Yield 42%.

IR (ATR) ν_{max}/cm^{-1}: 882-698 (ar**C-H** δ oop), 1560 (N-CO st sym, **NH_2** δ), 1592 (N-H δ, NH_2 amide and amine), 1632 (**C=O** st), 3082.6 (ar**C-H** st), 3314-3135 (**NH_2**st and **NH**val)

^{1}H NMR (500 MHz, [D_6]DMSO*δ*(ppm) (Figure S9): 1.17 (d, 6H, -CH(C**H_3**)**$_2$**); 2.07 (s, 3H, C**H_3**(cymene)); 2.74 (d, 3H, -NH-C**H_3**); 2.82 (m, 1H, -C**H**$(CH_3)_2$); 5.20 (s, 2H, -N**H_2**); 5.75 and 5.80 (m, 4H, C**H**(cymene)); 6.63; 6.89; 7.00 and 7.03 (dd, dd, t, t, 4H, C**H**(arene)) and 8.13 (d, 1H, N**H**).

^{13}C NMR (50 MHz, [D_6]DMSO*δ*(ppm) (Figure S10): 18.26 (-**C**H_3(cymene)); 21.90 (2C, -CH(**C**H_3)$_2$); 26.59 (-NH-**C**H_3) 30.37 (–**C**H$(CH_3)_2$); 85.91; 86.76; 100.49 and 106.79 (6C, (**C**H(cymene)); 113.20; 114.53; 116.68; 129.00; 135.89 and 148.96 (6C, **C**H(arene)) and 167.78 (**C**=O).

ESI/MS (m/z): negative mode 493 $[M+Cl]^-$ (calc.for $RuC_{18}H_{25}N_2OCl_3$ 491.6); positive mode 385$[M–2Cl]^+$ (calc. for $RuC_{18}H_{24}N_2O$ 385.1)

Elemental analysis: calculated for $RuC_{18}H_{24}N_2OCl_2$C, 47.35; H, 5.26; N, 6.14; found (%): C, 47.66; H, 5.50; N, 6.31.

3. Biological Studies

3.1. Cell Culture

MDA-MB-231 and MCF-7 cell lines were cultured in Dulbecco's modified Eagle's medium (DMEM) (Sigma-Aldrich Co), while HCC1937, MDA-MB-453, MDA-MB-361, and BEAS-2B cells were maintained in Roswell Park Memorial Institute (RPMI) 1640 nutrient medium (Sigma-Aldrich Co). All media were supplemented with 10% fetal calf serum (FCS) (pH 7.2) (Sigma-Aldrich Co), 2 mM L-glutamine, 25 mM 4-(2-hydroxyethyl)piperazine-1-ethanesulfonic acid (HEPES, Capricorn), and Penicillin-Streptomycin solution (Sigma-Aldrich Co) at a final concentration of 100 U/mL penicillin and 100 µg/mL streptomycin. To maintain HCC1937, MDA-MB-231, and MCF-7 cells, appropriate media were additionally supplemented with D-glucose (Sigma-Aldrich Co) to a final concentration of 4.5 g/L. Cells

were grown as a flat monolayer culture in tissue culture flasks (Thermo Scientific Nunc^{TM}), at a constant temperature of 37 ºC incubator with a humidified atmosphere of 5% CO_2.

3.2. MTT Assay

Impact of the novel ruthenium(II)-arene complexes (**C1**-**C4**), starting ruthenium(II)-arenes (**C5**, **C6**) and ligands (**L1**, **L2**), as well as reference compound cisplatin (*cis*-diamminedichloroplatinum(II), CDDP) on viability of cultured cells, was determined using the colorimetric 3-(4.5-dimethylthiazol-2-yl)-2.5-diphenyltetrazolium bromide (MTT, Sigma-Aldrich Co) assay, as previously described [69,70]. Cells were seeded in 96-well culture plates (Thermo Scientific Nunc^{TM}) at cell densities of 4000 c/w (MDA-MB-453), 6000 c/w (MDA-MB-231), 7000 c/w (BEAS-2B), 8000 c/w (MCF-7) and 10000 c/w (HCC1937, MDA-MB-361) in a total volume of 100 µL of nutrient medium, and then cultured in 37 ºC incubator for overnight. Stock solutions of investigated compounds were made prior to use in dimethyl sulfoxide (DMSO) at a concentration of 80 mM. The final concentration of DMSO did not exceed 1% (v/v) per well. The cells were subsequently treated with serial dilutions of freshly prepared ruthenium compounds and ligands (50 µM, 100 µM, 200 µM, 400 µM, and 800 µM) or cisplatin (6.25 µM, 12.5 µM, 25 µM, 50 µM, and 100 µM) in the nutrient medium. Upon continuous drug action for 72 h, 20 µL of MTT solution (5 mg/mL, Sigma-Aldrich Co) was added to each well and incubated with cells for 4 h at 37 ºC. Finally, to dissolve formed formazan crystals, 100 µL of 10% sodium dodecyl sulphate (SDS) was added to each well. Absorbances were read after 24 h on a microplate reader (ThermoLabsystemsMultiscan EX 200-240V) at 570 nm. The percentage of cell viability was calculated with the absorbance values of treated cells compared to the absorbance values of untreated cells (taken as 100%). IC_{50} values (concentration of investigated compound that reduced the number of viable cells in a treated cell population compared to a non-treated control to 50%) were determined by the correlation between the percentage of cell viability and the concentration of the drug after using the GraphPad Prism 6.0 software. Results are

eventually presented as the mean ±SD (standard deviation) and reported in µM. The selectivity index (SI) for tested compounds was calculated as the ratio: $SI_{HCC1937}$ (IC_{50} BEAS-2B/IC_{50} HCC1937), $SI_{MDA\text{-}MB\text{-}231}$ (IC_{50} BEAS-2B/IC_{50}MDA-MB-231), $SI_{MDA\text{-}MB\text{-}453}$ (IC_{50} BEAS-2B/IC_{50}MDA-MB-453), $SI_{MCF\text{-}7}$ (IC_{50} BEAS-2B/IC_{50}MCF-7), and $SI_{MDA\text{-}MB\text{-}361}$ (IC_{50} BEAS-2B/IC_{50}MDA-MB-361).Changes in HCC1937, MCF-7, and MDA-MB-231 cell morphology induced by investigated ruthenium(II)-arene complexes **C1**-**C4**, were evaluated by inverted microscopy (80x/0.2 objective), after 72 h of continuous drug treatment, before adding MTT solution.

3.3. Flow Cytometric Analysis of Cell Cycle Phase Distribution

HCC1937 cells were seeded in 6-well culture plates (Thermo Scientific Nunc^{TM}) in the nutrient medium at a density of 2.5 x 10^5 cells per well. After 24 h of growth, cells were continually exposed to ruthenium(II)-arene complexes (**C1**-**C4**), starting ruthenium(II)-arenes (**C5**, **C6**) and ligands (**L1**, **L2**) (200 µM and 500 µM), or to CDDP (5 µM and 10 µM). After 72 h incubation, cells were harvested by trypsinization, centrifuged, resuspended in phosphate-buffered saline (PBS), and fixed with 70% ice-cold ethanol at -20°C overnight. Flow cytometric analysis of the cell cycle phase distribution was performed in fixed HCC1937 cells after staining with propidium iodide (PI), as previously described [71,72]. Briefly, after fixation, cells were washed with cold PBS, incubated with 100 µg/mL of ribonuclease A (RNaseA; 1 mg/mL in PBS) for 30 min, and stained with 50 µg/mL of PI (400 µg/mL in PBS) in the dark, immediately before analysis. 10000 cells were collected for each sample and the cell cycle phase distribution was analyzed using a fluorescence-activated cell sorting (FACS) BD Calibur flow cytometer and Cell Quest computer software (Becton Dickinson, Heidelberg Germany).

3.4. Cellular Uptake, Subcellular Distribution and DNA Binding Studies

For cellular uptake, subcellular distribution, and DNA binding studies, 5 x 10^5 HCC1937 cells were grown in 25 cm^2 culture flasks (Thermo Scientific Nunc^{TM}) in triplicates. After 72

h, the nutrient medium was replaced with fresh medium containing 200 μM ruthenium(II)-arene complexes (**C1**-**C4**), and cells were incubated for another 24 h. The cells were harvested by trypsinization, and the cell pellet was collected by centrifugation at 1000 rpm for 7 min. Cell viability was determined by the Trypan blue exclusion assay. For subcellular distribution studies, the cell pellet was further lysed with the Subcellular Protein Fractionation Kit for Cultured Cells, according to the manufacturer's instructions (Thermo Scientific, cat.no.78840), providing five protein fractions: cytoplasmic, membrane, nuclear soluble, chromatin-bound, and cytoskeletal fraction. For DNA binding studies, total DNA from the HCC1937 cell pellet was isolated by using a salting-out procedure, as previously described [73,74]. The DNA concentration was determined by measuring the absorbance at A_{260}/A_{280} nm, with a BioSpec-nanospectrophotometer (Shimadzu Biotech). Measurements of total intracellular uptake, DNA binding, and accumulation in subcellular compartments of ruthenium(II)-arene complexes were performed in HCC1937 cells by using the inductively coupled plasma mass spectrometry (ICP-MS) and a Thermo Scientific iCAP Qc ICP-MS (Thermo Scientific, Bremen, Germany) spectrometer with Qtegra operational software [75]. The levels of ruthenium found in cells in total and in distinct cell compartments after the treatment were expressed as the amount of ruthenium (ng) taken up per 10^6 cells. The amount of ruthenium bound to the cellular DNA was expressed as pg of ruthenium per μg of DNA.

3.5. PARP-1Inhibitory Assay

Potential of examined ruthenium(II)-arene complexes (**C1**-**C4**) with benzamide ligands (**L1**, **L2**), as well as starting ruthenium(II)-arenes (**C5**, **C6**), for PARP-1 inhibition, was investigated by HT Universal Colorimetric PARP Assay (Trevigen, MD, USA, cat. no. 4677-096-K), according to the manufacturer's and previously reported instructions [76]. The kit measures the incorporation of biotinylated poly(ADP-ribose) onto histone proteins in a 96-well strip well format. 3-aminobenzamide (3-AB; provided in the kit) was used as control inhibitor. Briefly, the stock solutions of the investigated ruthenium compounds and ligands

were made in DMSO prior to use, and then serially diluted with 1 x PARP buffer to the required concentrations (1 µM, 10 µM, 100 µM, and 1000 µM). 3-AB was serially diluted with 1 x PARP buffer to the final concentrations of 1 µM, 10 µM, 100 µM, and 1000 µM. The tested compounds were incubated with PARP-1 (0.5 Units/well), biotinylated NAD^+, activated DNA, and histones that coated on the well. After incubation for 60 minutes at room temperature, the solution was subsequently removed, and streptavidin-horseradish peroxidase (Strep-HRP) was added for further incubation for 1 h. The final reaction was detected after incubation with pre-warmed TACS-Sapphire colorimetric substrate, in the dark, for 15 minutes at room temperature. The colorimetric reaction was stopped by the addition of 0.2 M HCl and ended in a yellow color stable for up to 1 h at room temperature. The absorbance was read at 450 nm on a microplate reader (ThermoLabsystemsMultiscan EX 200-240V). The differences in colour intensities reflect the PARP-1 inhibition efficiencies of the tested compounds. By taking into account activity controls (without inhibitor) and negative controls (without PARP-1), the monitored mean optical density values were converted into relative values corresponding to the respective percentage of PARP-1 inhibition. From a plot of compound concentration *versus* the percentage of PARP-1 inhibition obtained from the GraphPad Prism 6.0 software, IC_{50} values were determined for 50% PARP-1 inhibition.

3.6. Agarose Gel Electrophoresis Assay

The interaction of ruthenium(II)-arene complexes (**C1**-**C4**), starting ruthenium(II)-arenes (**C5**, **C6**) and ligands (**L1**, **L2**), as well as CDDP, with pHOT-1 plasmid DNA, was studied by agarose gel electrophoresis [77]. 300 ng of pHOT-1 plasmid DNA (3.3 µg/µL) was incubated with ruthenium compounds and ligands (200 µM and 400 µM), or CDDP (12.5 µM, 25 µM, 50 µM, and 100 µM) for 24 h, at 37 °C in 5 mMTris-HCl/50 mMNaCl buffer (pH 7.2). The experiments were also carried out in the presence of 100 µM DAPI (4′,6-diamidino-2-phenylindole; minor groove binder) or MG (methyl green; major groove binder), which were added to the pHOT-1 plasmid DNA 1 h prior to the addition of investigated

ruthenium complexes **C1**-**C4**. The final solutions were incubated 24 h. The samples were then analysed by 0.8% agarose gel electrophoresis in 1 x TBE (Tris-borate-EDTA) buffer (pH 8.0) for 2 h, at 30 V. After electrophoresis, the gel was stained for 1 h by soaking it in an aqueous GelRed solution, and subsequently visualized by UV transilluminator.

4. Results and Discussion

4.1. Synthesis and Characterization

Four new ruthenium(II)-arene complexes (**C1**-**C4**) were synthesized in the reaction of 3-aminobenzamide analogues, 2-amino-4-methylbenzamide (**L1**) and 3-amino-N-methylbenzamide (**L2**), to get potentially good PARP inhibitors (Scheme 1). Starting Ru(II) complexes were Ru(II) dimmers with toluene or *p*-cymene moiety. Synthesis of Ru(II)-*p*-cymene-based complexes with **L1** and **L2** has to be done in an oxygen-free atmosphere, as it was previously reported for similar complexes [65]. All syntheses were performed in methanol solution. Yellow-orange complexes with **L2** precipitated during the reaction, while complexes with **L1** precipitated exclusively after the addition of an excess of NH_4PF_6. Spectral and conductivity measurement data confirmed that ligand **L1** bound bidentately, via both of nitrogen atoms, while ligand **L2** was monodentately coordinated to the metal ion.

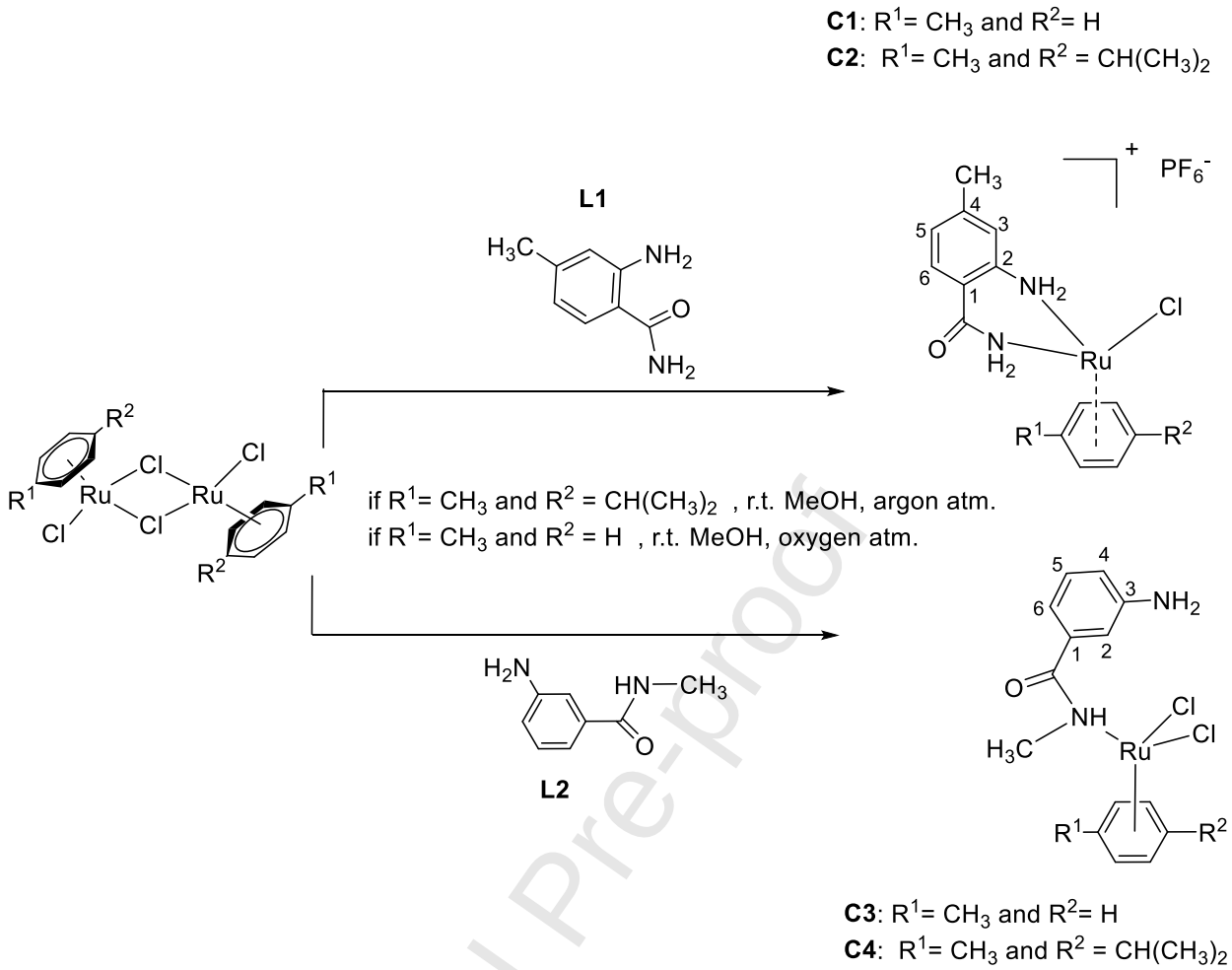

Scheme1. Reaction scheme describing the synthesis of the **C1**-**C4** complexes.

4.1.1. IR Spectroscopy

Broad, intensive band from 3406 to 3168 cm^{-1}, corresponding to NH_2 amine and amide standard vibrations in ligand **L1** became sharper and moved to lower wave number values in complexes and **C2**, due to coordination to metal ion via these two nitrogen atoms. Band for N-C amide standard symmetrical vibration at 1615 cm^{-1} was moved to 1534 and 1549 cm^{-1} for complexes **C1** and **C2**, respectively. NH_2 deformation vibration bands appeared in both complexes at 1565 cm^{-1}, compared to ligand at 1548 cm^{-1}, due to coordination via amine nitrogen atoms.

There were changes in shape, and slightly in wave numbers in IR spectra of complexes **C3** and **C4**, in the area from 3300 to 3100 cm^{-1}, which could be confirmation for coordination via

amide nitrogen atom. Sharp, very well defined and intensive bands of standard symmetric N-C and NH amide deformation vibrations appeared at 1563 and 1598 cm^{-1},compared to less intensive and broader bands at 1559 and 1592 cm^{-1}, in the ligand IR spectrum. These changes in wave numbers and shape were the consequence of amide nitrogen atom coordination to the metal ion.

4.1.2. NMR Spectroscopy

4.1.2.1. ^{1}H NMR Spectroscopy

Firstly of all, for complexes **C1** and **C2**, we could see little upfield changes in ^{1}H NMR spectra for a signal corresponding to amide protons (two singlets at 7.59 and 6.90 ppm for complex **C1**; 7.64 and 6.95 ppm for complex **C2**). Well defined, separated signals for amine protons (6.52 ppm), and proton from C3 carbon in aromatic ring (6.47 ppm),were noticeable in the ^{1}H NMR ligand **L1** spectrum. These signals are closer to each other, and formed a multiplet signal at 6.47 to 6.59 ppm in complex **C1** and a broad singlet at 6.52 ppm in the ^{1}H NMR **C2** spectrum. Changes in the chemical shift values in observed ^{1}H NMR spectra of ligand and complex pointed to the bidentately coordination via both of the nitrogen atoms in ligand moiety. There were also noticeable changes of chemical shift values for protons in arene cap in synthesized Ru(II)-arene complex comparing to starting Ru(II) arene dimers. For these protons in toluene moiety, we could see changes in the shape of signals, as well as the division of one signal to two separated signals (signal corresponding to two protons from C3 and C5 are moved from 5.98 ppm (**L1**) to 6.00 and 6.15 ppm (**C1**). In cymene-based Ru(II) complex, **C2**, we could see broad doublet from 5.81 to 5.78 ppm for four aromatic protons. (Figure S3). In^{1}H NMR spectra of **C1** and **L1** recorded in d_4-CD_3OD were very well noticeable changes in chemical shifts values for all protons, but because of proton exchange between ligand and solvent, we could not see amide and amine protons. Signals for all protons from ligand moiety were shifted downfield in ^{1}H NMR spectrum of **C2** corresponding to ligand: C6, 1H from 7.41 to 7.66 ppm, C3, 1H from 6.56 to 7.47 ppm, C5

1H from 6.45 to 7.22 ppm and finally signal for methyl group protons from 2.22 to 2.50 ppm. Signal for protons from cymene moiety was observed in the region from 5.29 to 5.56 ppm (aromatic) and methyl and isopropyl groups at 1.89, 2.60 and 1.20 ppm, respectively (Figure S6).

In the ^{1}H NMR spectra of complexes **C3** and **C4**, we could see upfield changes of the signal corresponding to the amide proton (from 8.15 ppm in **L2** to 8.04 ppm in complexes). Also, signals for all other protons in complex **C3** had slightly lower values, as a result of ligand coordination to ruthenium(II) ion. As it was expected, signals for toluene or cymene protons were at lower chemical shifts than in corresponding ruthenium(II) dimers. In this complex, it is also supposed that the coordination to a metal ion is via amide proton, based on changes in chemical shifts in complexes compared to ligand itself.

4.1.2.2. ^{13}C NMR Spectroscopy

There were no significant changes in the ^{13}C NMR spectra of synthesized complexes, compared to the ligand spectrum, recorded in d_6-DMSO. Characteristic signals for carbon atom from carbonyl group were around 171 ppm, signals for arene carbon atoms from ligand moiety were in the area from 150 to 111 ppm, while toluene or cymene arene carbon atoms gave signals from 105 to 82 ppm or 96 to 85 ppm, respectively. Signal for carbon atom from ligand methyl group appeared around 21 ppm in ^{13}C NMR spectrum of ligand, as well as in both spectra of complexes. Below 30 ppm, signals appeared for carbon atom from the toluene methyl group (~ 22 ppm), and carbon atoms from cymene isopropyl group (**C**H ~ 30 and 2**C**H_3 ~ 18 ppm).

All signals for aromatic carbon atoms from ligand were moved little upfield in the d_4-CD_3OD spectrum of complex **C2**. Signals for cymene aromatic carbon atoms appeared also in the region from 96 to 82 ppm, and methyl group carbon atoms signals are placed at 22.55 (from ligand) and 17.86 (from cymene), while isopropyl carbon atom signal appeared at 32.09 ppm.

In the ^{13}C NMR spectrum of ligand and corresponding complexes **C3** and **C4**, we could see changes in chemical shift values, which were a little bit higher in complexes compared to the ligand. We could see changes in chemical shift value for the carbonyl group, which was one more confirmation for amide proton coordination to Ru(II) ion.

4.1.2.3. Chemical behaviour of the Ru(II)-arenes in DMSO

Stability of Ru(II)-arenes in the most commonly used solvents for biological assay experiments, water or DMSO, is studied and become important data for explaining biological activity of potentially new metallodrugs [78]. Some of these studies showed that N or O donor ligands or even arene cap have been replaced with DMSO [79]. In order to investigate behaviour of synthesized Ru(II)-arene compounds (C1-C4), we followed ^{1}H NMR spectral changes in complex solutions in deuterated DMSO during 72 hours (at 0h, 24h, 48h and 72h after dissolution). These spectra showed traces of free arene (cymene or toluene) after 24h followed by slow increasing of its amount in solution (11% after 72h, Figure S11). Since, the solutions of complexes used in biological tests were prepared immediately prior to use, and that final concentration of DMSO did not exceed 1% in total media, we can assume that significant changes in complex structure were not occurred.

4.1.3. Mass Spectrometry

Mass spectra of synthesized complexes show characteristic bands in negative as well as in positive mode. For complexes **C1** and **C2** we could not detect molecular ion but we could see two type of peaks in negative mode, for $[M\text{-}PF_6\text{-}H]^-$ ion and $[M\text{-}PF_6\text{+}Cl]^-$, till in positive recording mode peaks for $[M\text{-}PF_6\text{-}Cl]^+$ ions were detected. In the mass spectra of **C3** and **C4** complexes we could detect peaks for $[M+Cl]^-$ and $[M-H]^-$ ions in negative, as well as peaks for $[M\text{-}2Cl]^+$ ions in positive recording mode.

4.1.4. Conductivity Measurements

Molar conductivity measurements were done to get additional confirmation of complexes structure. All complexes were well soluble in dimethyl sulfoxide (DMSO), so we used 1mM solutions in this solvent for conductivity measurements. For complexes **C1** and **C2**, conductivity values were 22.7 Ω^{-1} cm^2 mol^{-1} and 24.3 Ω^{-1} cm^2 mol^{-1}, respectively, and for complexes **C3** and **C4**, 1.65 Ω^{-1} cm^2 mol^{-1} and 3.46 Ω^{-1} cm^2 mol^{-1}, respectively. From the observed values, we could confirm that complexes **C1** and **C2** correspond to 1:1 electrolyte type, as well as that molar conductivity measurement values for **C3** and **C4** correspond to neutral complexes [80].

4.1.5. Hydrolysis of synthesized complexes (Cl/H_2O exchange process)

The mechanism of cytotoxic action of Ru-arene complexes of the type $[Ru(\eta^6\text{-arene})(XY)(Z)]_n^+$ (where XY = chelating ligand and Z = labile halide), is generally thought to involve hydrolysis of the Ru−Z bond, generating an active Ru−OH_2 species. Depending on pH values, Ru−OH_2 and Ru−OH species will be present, and in different ratios. Certainly, hydrolysis can be suppressed extracellularly due to high [Cl^-] but becomes possible after the complex enters the cells because of a lower intracellular [Cl^-] [81]. The hydrolysis rates of complexes may vary over many orders of magnitude [82]. Here we followed time dependence of H_2O/Cl exchange process by UV-Vis spectroscopy. Initial solution was 2mM solution of C3 in H_2O at pH 6.8. For this type of Ru(II) complex at this pH, Ru−OH_2 is the most abounded specie. Then we added solution of KCl with final concentration of 100 mM, 24 mM and 4 mM (imitating blood plasma, cytoplasm and cell nucleus). In all cases there were changes in UV-Vis spectra before and immediately after adding the KCl. Further changes in spectra during the time have not been observed. So, we can conclude that this reaction was completely immediately, there were no time dependence, reaction is fast.

The work of Sarah J. Dougan and Peter J. Sadler reviewing the comparative aqueous solution chemistry, cancer cell cytotoxicity and reactivity towards different biomolecules for these

type of complexes containing various arenes, chelating ligands, and monodentate leaving groups clearly showed that the variations in identity of all three groups of ligands may tremendously influence the pharmacological properties of these complexes [81]. This observation was confirmed in several papers; our previous work with similar organoruthenium(II) complexes containing the *p*-cymene ligand and a pyridine derivative coordinated in a monodentate or bidentate manner imply that there is no simple correlation between fast hydrolysis of complexes, high-yield reaction with 9-methyladenine, and inhibition of tumor cells growth [83]. The unique combination of ligands determines the unique mechanism of activation and cytotoxic action, which must be an integral part of the investigation of novel ruthenium complexes. For complexes investigated in this work remains to be further thoroughly examined coordination to enzymes, DNA, or other cell constituents/different biomolecules.

4.2. PARP-1 Inhibition

To investigate the inhibitory potential on PARP-1 enzymatic activity of four novel ruthenium(II)-arene complexes (**C1**-**C4**) with benzamide ligands (**L1**, **L2**), we used Trevigen´s HT Universal Colorimetric PARP Assay Kit, that measures incorporation of biotinylated poly(ADP-ribose) onto histone proteins *in vitro*. The inhibitory effects of novel complexes, their starting complexes (**C5**, **C6**) and the deriving ligands (**L1**, **L2**), were compared to determine whether the incorporated benzamide ligands or the arene ligands (*p*-cymene *versus* toluene) may contribute to the PARP-1 inhibitory potency of the resulting Ru(II) complex. 3-AB was used as a positive reference compound. The results in term of IC_{50} values determined for 60 minutes incubation *in vitro* are presented in Table 1. Although the literature value of the 3-AB (33.8±2.2 μM) was nicely reproduced [84], benzamide derivatives, **L1** and **L2**, exhibited significantly lower PARP-1 inhibitory activity (IC_{50}>1000 μM), providing only 23.6% and 25.5% of PARP-1 inhibition at 1000 μM, respectively. As

expected, four novel ruthenium(II)-arene complexes displayed inhibitory effects, with IC_{50} values in the range from 25.5-709.7 μM. All complexes, except **C3**, showed similar concentration-dependent PARP-1 inhibitory activity and reached maximum effect (100% inhibition) at 1000 μM. Complexes with *p*-cymene moiety, **C2** and **C4**, emerged as superior PARP-1 inhibitors (IC_{50} values being 25.5 μM and 29.4 μM, respectively) to complexes with toluene moiety, **C1** and **C3** (IC_{50} values being 50.2 μM and 709.7 μM, respectively). Additionally, **C2** and **C4** exhibited lower IC_{50} values against PARP-1 than 3-AB. Furthermore, starting ruthenium(II)-*p*-cymene complex, **C6**, showed to be approximately 8-times more potent in inhibiting PARP-1 (IC_{50}=40.4±6.4 μM) than ruthenium(II)-toluene complex, **C5** (IC_{50}=321.9±92.6 μM).

Table 1. PARP-1 inhibitory activities of investigated ruthenium complexes (**C1**-**C4**), ruthenium(II)-arenes (**C5**, **C6**), ligands (**L1**, **L2**), and 3-AB following 60 minutes incubation *in vitro*.

Compound	PARP inhibition (%)				PARP inhibition (μM)
	1	10	100	1000 (μM)	IC_{50}[a] (mean ± SD)
C1	1	2.6	82.5	100	50.2±3.9
C2	8.5	21.8	85.9	100	25.5±0.2
C3	-0.2	1.4	12.7	58.5	709.7±92.2
C4	5.3	27.2	74.8	100	29.4±5.9
C5	2.4	5.8	24.2	75	321.9±92.6
C6	17.8	34.7	56	86.3	40.4±6.4
L1	3.1	10.9	13.9	23.6	>1000[b]
L2	8.2	10.2	19.3	25.5	>1000[b]
3-AB	20.5	26.1	64.3	98.5	33.8±2.2

[a]IC_{50} values are expressed as the mean ± SD of at least duplicate determinations.[b]>1000 denotes that IC_{50} was not obtained in the range of concentrations tested up to 1000 μM.

From a general structure-activity standpoint, complexes with bidentate coordinated ligand (**C1** and **C2**) demonstrated higher efficacy in inhibiting PARP-1, comparing to the other two complexes (**C3** and **C4**). In addition, complexes carrying *p*-cymene (**C2** and **C4**) presented as better PARP-1 inhibitors than complexes carrying toluene (**C1** and **C3**). This implies that

structural variations influence the specificity and potency of complexes to inhibit PARP-1 activity. Data obtained were in accordance with the previous reports on PARP-1 inhibitory potential of ruthenium(II)-arenes (RAPTA-T with toluene moiety [66] and series with *p*-cymene [65]). The present study, to the best of our knowledge, for the first time included starting binuclear ruthenium(II)-arene complexes **C5-C6**. Ruthenium(II)-*p*-cymene scaffold could be distinguished as the perspective for further structural improvements, and investigation of PARP-1 inhibitory potential. The stronger PARP-1 inhibitory activity of bidentate conjugate molecules **C1** and **C2,** also correlated to their generally higher antiproliferative effects (see below).

4.3. Cell Growth Inhibition

The cell growth inhibition of four new ruthenium(II)-arene complexes, as well as their corresponding starting binuclear ruthenium(II) complexes and ligands, was assessed on a panel of five human breast cancer cell lines (HCC1937, MDA-MB-231, MDA-MB-453, MDA-MB-361, MCF-7) and one human non-cancer bronchial epithelium cell line (BEAS-2B), utilizing an MTT assay, with cisplatin (*cis*-diamminedichloroplatinum(II), CDDP) used as a reference compound. Genotype and phenotype characteristics of breast cancer cell lines used in this study [85-87] are summarized in Table 2. While HCC1937, MDA-MB-231, and MDA-MB-453 cell lines are considered as triple-negative breast cancer cells (or hormone-insensitive), MCF-7 and MDA-MB-361, are positive for estrogene and progesterone receptors, and therefore described as hormone-sensitive. In this breast cancer cell lines panel, only HCC1937 cells are homozygous for the *BRCA1* 5382insC mutation and experience a complete loss of BRCA1 function [88], while other investigated breast cancer cells have wild-type *BRCA1* gene expression.

Table 2. Characteristics of breast cancer cell lines used in the current study.

Property	**HCC1937**	**MDA-MB-231**	**MDA-MB-453**	**MCF-7**	**MDA-MB-361**
Tumor classification	BaA	BaB	HER2/neu amplified	Lu	Lu

ER/PR/(HER2/neu overexpression)	-/-/-	-/-/-	-/-/- *	+/+/-	+/-/+
BRCA1	MUT (hom, 5382insC)	WT	WT	WT	WT
TP53	MUT **	MUT (hom)	WT	WT	WT
Other mutated genes	PTEN (hom del)	BRAF (het), CDKN2A (hom), KRAS (het), NF2 (hom)	CDH1 (hom), PIK3CA (het), KRAS	CDKN2A (hom), PIK3CA (het act mut)	CDKN2A (hom), PIK3CA (het)
Tumor source	P	M (Pl.E)	M (Pc.E)	M (Pl.E)	M (Br)
Tumor type	TNM stage IIB, grade 3, IPDC	AC	AC	IDC	AC
Morphology	E	ML (highly metastatic)	E	E	E
Tumorigenicity	yes	yes	no	yes	yes

Abbreviations: BaA, BasalA; BaB, BasalB; HER2, human epidermal growth factor receptor 2; Lu, Luminal; ER, estrogen receptor; PR, progesterone receptor; MUT, mutant gene; WT, wild-type gene; hom, homozygous; het, heterozygous; del, deletion; act mut, activating mutation; P, primary; M, metastasis; Pl.E, pleural effusion; Pc.E, pericardial effusion; Br, brain; IPDC, infiltrating primary ductal carcinoma; AC, adenocarcinoma; IDC, invasive ductal carcinoma; E, epithelial; ML, mesenchymal-like. *For MDA-MB-453, *HER2/neu* is amplified, but not highly expressed. **For HCC1937, acquired mutation in TP53 gene with wild-type allele loss.

The two ligands, **L1** and **L2**, showed very low cell growth inhibition potential, against all tested cells, and were nontoxic even at a concentration up to 800 μM (Table 3). However, when coordinated to the ruthenium(II)-arene moieties, resulting complexes, **C1**-**C4**, displayed cell growth inhibition potential, with IC_{50} values in the micromolar range: 146.9-580.5 μM. Precursor ruthenium(II)-arenes, **C5** and **C6**, exhibited IC_{50} values varying from 130.6 μM to 418 μM.

Table 3. Cell growth inhibitory activity of investigated ruthenium complexes (**C1**-**C4**), ruthenium(II)-arenes (**C5**, **C6**), ligands (**L1**, **L2**), and CDDP expressed through IC_{50}[a] values (μM) obtained by MTT assay after 72 h of continuous drug action.

Compound	HCC1937	MDA-MB-231	MDA-MB-453	MCF-7	MDA-MB-361	BEAS-2B	$SI_{HCC1937}$[c]	$SI_{MDA-MB-231}$[c]	$SI_{MDA-MB-453}$[c]	SI_{MCF-7}[c]	$SI_{MDA-MB-361}$[c]
C1	153.6	173.8	554.5	146.9	429.2	227	1.48	1.3	0.41	1.55	0.53
C2	428.1	196.9	580.5	156.6	406	452	1.06	2.3	0.78	2.88	1.11
C3	235.9	309	489.9	270.5	464.6	349.9	1.48	1.13	0.71	1.29	0.75
C4	315.8	364.9	446.8	309.5	439.9	355.2	1.12	0.97	0.79	1.15	0.81
C5	194.9	178.2	382.7	130.6	411.7	202.1	1.04	1.13	0.53	1.55	0.49
C6	130.8	222.6	343.7	168.7	418	174.1	1.33	0.78	0.51	1.03	0.42
L1	>800[b]	>800[b]	>800[b]	>800[b]	>800[b]	>800[b]	–[d]	–[d]	–[d]	–[d]	–[d]
L2	>800[b]	>800[b]	>800[b]	>800[b]	>800[b]	>800[b]	–[d]	–[d]	–[d]	–[d]	–[d]
CDDP	10.7	7.1	10	5.6	26	4.8	0.45	0.62	0.48	0.85	0.18

[a] IC_{50} values (μM) are expressed as the mean ± SD of at least two independent experiments performed in triplicate (SD values were lower than 15 in all measurements for complexes and ligands, while for CDDP values were lower than 1 in all measurements). [b] >800 denotes that IC_{50} was not obtained in the range of concentrations tested up to 800μM. [c] The selectivity index (SI) for tested compounds was calculated as described in the Methods section.[d] "–" stands for not determined.

Differences observed in the sensitivity pattern among breast cancer cell lines treated with the investigated complexes **C1**-**C4**, most probably emerged due to the genetic and phenotypic variations between the cells. Generally, higher sensitivity to the action of **C1**-**C4** was found in HCC1937, MDA-MB-231 and MCF-7 cells, which displayed some similarities in response, as seen from the cell survival curves (Figure S12). Hormone-responsive MDA-MB-361 cells showed approximately equal low sensitivity to **C1**-**C6**. Structure-activity comparison indicated that complexes with bidentately bond benzamide ligand, **C1** and **C2**, exhibited lower IC_{50} values, than complexes **C3** and **C4**, with monodentate ligand, except in HCC1937 cells, where **C2** was the least active, with IC_{50}=428.1±12.5 μM.

In summary, antiproliferative efficiency of **C1**-**C4** in HCC1937cells, decreases in the following order: **C1**>**C3**>**C4**>**C2**, and in MDA-MB-231 and MCF-7 cells, as follows: **C1**>**C2**>**C3**>**C4**. Results pointed out the highest activity of **C1** in HCC1937, MDA-MB-231,

and MCF-7 cells, with IC_{50} values being 153.6 μM, 173.8 μM, and 146.9 μM, respectively. The corresponding values for selectivity index (SI) (Table 3) were: 1.48, 1.3 and 1.55, respectively, as determined according to the response in non-malignant BEAS-2B cells. Complex **C2** also displayed 2.3- and 2.88-fold higher cytoselectivity toward MDA-MB-231 and MCF-7 cells, respectively.

Cisplatin showed IC_{50} in the low micromolar range of 5.6-26 μM (Table 3), with the highest activity toward MCF-7 cells (IC_{50}=5.6±0.5 μM), and the lowest toward MDA-MB-361 cells (IC_{50}=26 μM). The response of triple-negative breast cancer cells from this panel to cisplatin treatment was approximately in the same line of concentrations (IC_{50}~ 10 μM).

It is of importance to note, that antiproliferative effects of **C1**-**C4** in the tested panel of cell lines cannot be ascribed only to their PARP-1 inhibitory effects. Despite the observed potency for PARP-1 inhibition, complexes **C2** and **C4** displayed weak cell growth inhibition in HCC1937, MDA-MB-231, and MCF-7 cells. The cytotoxicity range (observed through IC_{50} values *in vitro*) of C1 - C4 complexes is within well-known ruthenium complexes, such as RAPTA compounds, and especially NAMI-A, which showed to be weakly cytotoxic in vitro, even at a concentration up to 500 μM [65, 66]. In the case of NAMI-A, we saw that high cytotoxicity is not a prerequisite for further development of a compound as an anticancer drug candidate. Although being essentially non-toxic to primary cancer cells, NAMI-A exhibits antimetastatic activity [89]. Additionally, RNA-seq analysis of the whole transcriptome of metastatic versus non-tumorigenic cells exposed to NAMI-A by Sava *et al* revealed a pharmacological signature in good agreement with the NAMI-A behavior as a metastasis inhibitor, confirming its selectivity towards cell populations with metastatic features [90]. Additional structure-activity studies were performed to reveal possible multi-targeting properties of complexes **C1-C4**, and the mechanism of action in HCC1937 breast cancer cells. This cell line was interesting for further research, as already mentioned, because of its homozygous mutation in the *BRCA1* gene and complete loss of BRCA1 function,

supporting its good response to PARP inhibitors, in a synthetic lethality manner [35, 91]. But, we must note that, according to the literature data [92], additional genetic alterations may accumulate, such as loss of *PTEN*, gene that is frequently mutated in *BRCA1*-deficient breast cancers (see Table 2) [93], that, in turn, restore HR repair efficiency. We must have all of this in mind, as well as complexity of the topic, in our effort to explain the poor selectivity of investigated complexes **C1**-**C4**. Moreover, MDA-MB-231 and MCF-7 breast cancer cells, despite being *BRCA1/2* wild-type, may harbour HR deficient phenotype [94,95], that renders them sensitive to PARP inhibitors. Together, these data support our findings of cell line-dependent biological activity of tested ruthenium complexes in breast cancer cell line panel.

4.4. Impact on Cell Morphology

Since the MTT assay relies mostly on the measurement of the mitochondrial dehydrogenase activity, obtained results expressed in terms of IC_{50} values, cannot distinguish among cytotoxic and antiproliferative effects of the tested drug [96]. The morphological appearance of cells can give valuable information about concentration- and time-dependent changes in cell response. The examination of morphological changes in HCC1937, MDA-MB-231 and MCF-7 cell lines, following **C1**-**C4** action (72h) (Figure 3 and Figure S13), revealed a concentration-dependent reduction in the number of cells. Treatment of MCF-7 cells with 400 μM complexes **C1**-**C4** caused the appearance of a mixed cell population of rounded cells, and cells with preserved morphology (Figure S13A). More pronounced changes in cell density and morphology were caused at higher concentrations (800 μM) of **C1** and **C2**. MDA-MB-231 cells showed a similar response, though followed with cell elongation and the appearance of pseudopods (Figure S13B).

In HCC1937 cells, **C1**-**C4** caused a dose-dependent decrease in cell number, along with the appearance of small rounded cells, and individual enlarged single- or multi-vacuolated cells, already at 200 μM treatment (Figure 3). At 800 μM, complexes profoundly altered HCC1937 cell morphology, promoting the appearance of a bigger portion of rounded cells, indicative of

cell death. The majority of HCC1937 cells treated with **C1** became rounded and formed clusters. All together, these findings support results of MTT study which indicated higher cell growth inhibitory potential of complex **C1**, than its structurally-related **C2**-**C4** complexes.

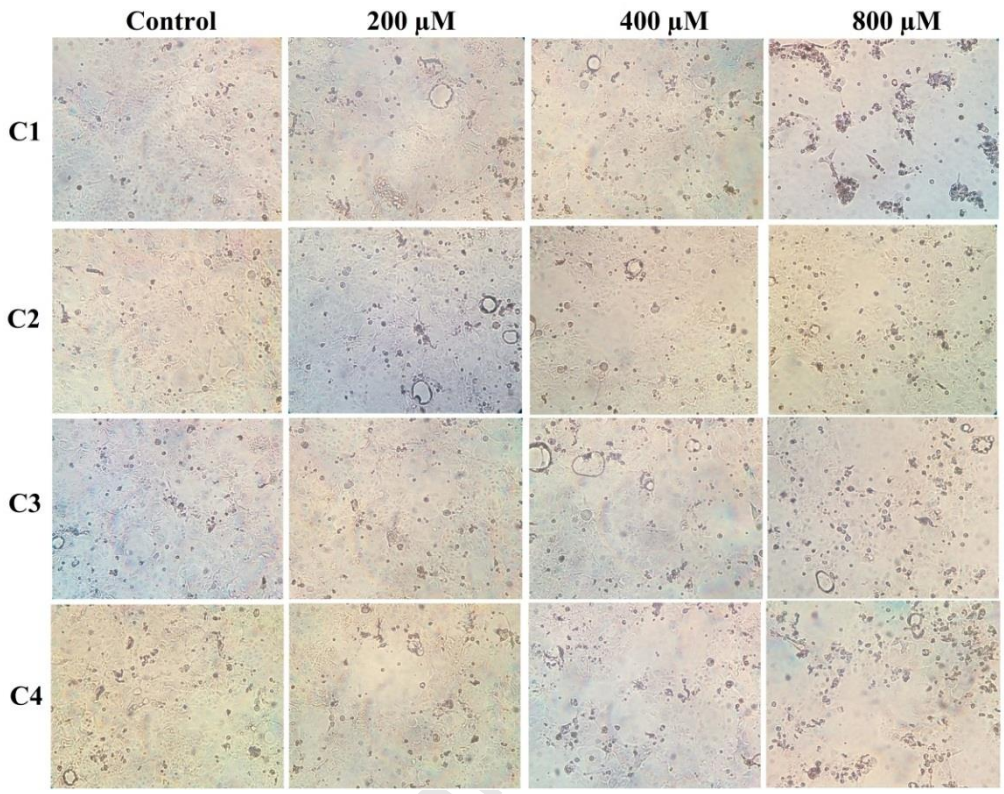

Figure 3. Photomicrographs of HCC1937 control cells and cells exposed to 200 µM, 400 µM, and 800 µM ruthenium complexes (**C1**-**C4**) for 72 h. Cells were observed under the bright filed inverted microscope, using the 80x/0.2 objective.

4.5. Cell Cycle Arrest

The effect of investigated compounds on cell cycle progression in HCC1937 cells was analysed by flow cytometry. After 72 h of treatment with ruthenium complexes and ligands (200 µM and 500 µM), or CDDP (5 µM and 10 µM), the DNA content in cells was estimated by PI staining. The data are presented in Figure 4. Treatment with 5 µM of CDDP induced significant arrest of the cell cycle in the G2-M phase (up to 54.2%, *versus* 20.8% in control). Increasing concentration of CDDP to 10 µM triggered accumulation in the S phase of the HCC1937 cell cycle up to 34.5%, compared to 21.3% in control (Figure 4 and Figure S14). Treatment with ligands **L1** and **L2** did not induce any significant changes in the cell cycle

phase distribution, for 72 h drug action, at two tested concentrations (treatment with 200 µM, data not shown). Among investigated ruthenium complexes, only **C5** (binuclear complex with toluene as arene) and novel **C1**, applied at 500 µM, induced evident changes in the cell cycle of HCC1937 cells (Figure 4). **C5** caused arrest of the cell cycle in the S phase (up to 32.1%, *versus* 21.3% in control), and accompanying decrease of percent of cells in the G1 phase (up to 38.0%, *versus* 55.5% in control). Negligible increase was detected in the HCC1937 Sub-G1 region, characteristic for fragmented DNA and apoptotic cells, after **C5** and **C6** treatment. **C1**-induced S phase arrest in the *BRCA1*-mutated HCC1937 cells (up to 28.5%, compared to 21.3% in control) suggested capability of this compound to block DNA replication. This effect can be related to the same ability of its constituted ruthenium(II)-toluene, **C5** [21]. Present results are in good correlation with the data showing DNA binding potential of ruthenium(II), obtained by ICP-MS (see below). It is most likely that the highest activity of **C1** in HCC1937 cells is due to the more efficient cell cycle arrest.

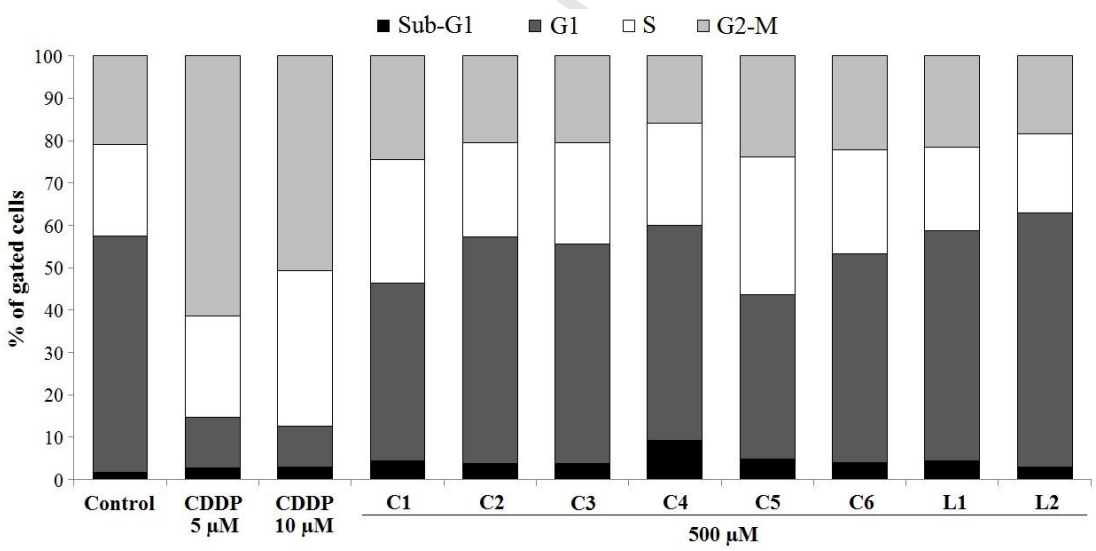

Figure 4. Flow cytometric analysis of the HCC1937 cell cycle phase distribution in response to the 72 h treatment with 500 µM ruthenium complexes (**C1**-**C4**), ruthenium(II)-arenes (**C5**, **C6**), and ligands (**L1**, **L2**), or with 5µM and10µMCDDP. Results are representative of at least two independent experiments and displayed as a diagram showing the percentage of cells in each cell cycle phase out of 10000 analyzed cells.

4.6. Differential Cellular Accumulation

To further investigate the mechanism underlying the activity of **C1**-**C4** complexes in HCC1937 cells, and to locate their possible targets in the cell, total cellular uptake and subcellular distribution studies have been performed by ICP-MS. The affinity of **C1**-**C4** for DNA binding was determined according to the ruthenium(II) content (pg Ru/μg DNA) found in the genomic DNA, isolated from treated HCC1937 cells. The results shown in Figure 5 revealed that after 24 h of continual treatment with equimolar concentrations (200 μM), all four complexes entered the HCC1937 cells, and accumulated in different amounts. **C1**-**C4** can be arranged in decreasing order, according to the intracellular content (ng Ru/10^6 treated cells), as following: **C1**>**C3**>**C4**>**C2** (Figure 5A). **C1** entered the HCC1937 cells most efficiently and reached a concentration of 85.6±0.2 ng of Ru in 10^6 cells. **C2** showed the lowest ability to enter the HCC1937 cells since there was only 21.6±0.1 ng of Ru found in 10^6 cells. A similar trend was observed in the DNA binding affinity of complexes. Results revealed 3.8-fold higher amount of **C1** (39.2±0.6 pg of Ru per μg of DNA) than **C2** (10.2±0.1 pg of Ru per μg of DNA), in the DNA fraction of HCC1937 cells (Figure 5B). The ICP-MS analysis of compounds distribution through cellular compartments, disclosed a similar localization pattern of **C1**, **C3**, and **C4** in HCC1937 cells (Figure 5C). These three complexes accumulated at the highest amount in the cytosol (71.5%, 67.1%, and 68.6%, respectively), and in some lower amount in the membrane/organelle fraction of treated cells (19.3%, 27.2%, and 27.1%, respectively). On the contrary, **C2** retained in the membrane/organelle fraction as the largest portion (49.1%), and to the lower extent in the cytosol (40.8%). Furthermore, significant ruthenium content was found in the nuclear fraction (both soluble and chromatin-bound nuclear fraction) of HCC1937 cells treated with **C1**-**C4**, i.e. 7.5%, 6.8%, 4.5%, and 4.1%, respectively. Only a small amount of ruthenium atoms was found in the cytoskeletal fraction (1.7% from **C1**, 3.3% from **C2**, 1.2% from **C3**, and 0.2% from **C4**).

Drug localization in the specific cellular compartment, and therefore interaction with its biomolecules, is not only structure-dependent, but also time- and concentration-dependent, as

reported for different ruthenium complexes [97,98]. According to the data obtained and structure-activity correlations, it is notable that complex **C1**, of structural formula [(η^6-toluene)Ru(**L1)**Cl]PF_6, carries an advantage over the rest of tested complexes, in the ability to enter the cell and bind to nuclear DNA. The highest intracellular uptake of **C1**, and accompanying accumulation in the DNA fraction of HCC1937 cells, are well in accordance with the higher growth inhibitory activity of this compound. Additionally, notable **C1** accumulation in the nuclear fraction of cells may point to the tendency of this type of "combi-molecules" [63] to also interact with DNA-associated proteins, such as PARP-1. This is in accordance with the PARP-1 inhibitory potential of **C1** observed in the present study, and as well as with the previous reports of cellular uptake of some ruthenium(II)-arene complexes with phenanthridin-based ligands [65].

Lower intracellular content of **C2**, **C3**, and **C4** could be explained either by reduced uptake or enhanced efflux of these compounds, which favours their lower growth inhibitory activity. Preferential uptake of **C1** by HCC1937 cells emphasizes that structural differences between investigated ruthenium complexes significantly influence affinity and stability of interactions with cellular proteins and nuclear DNA.

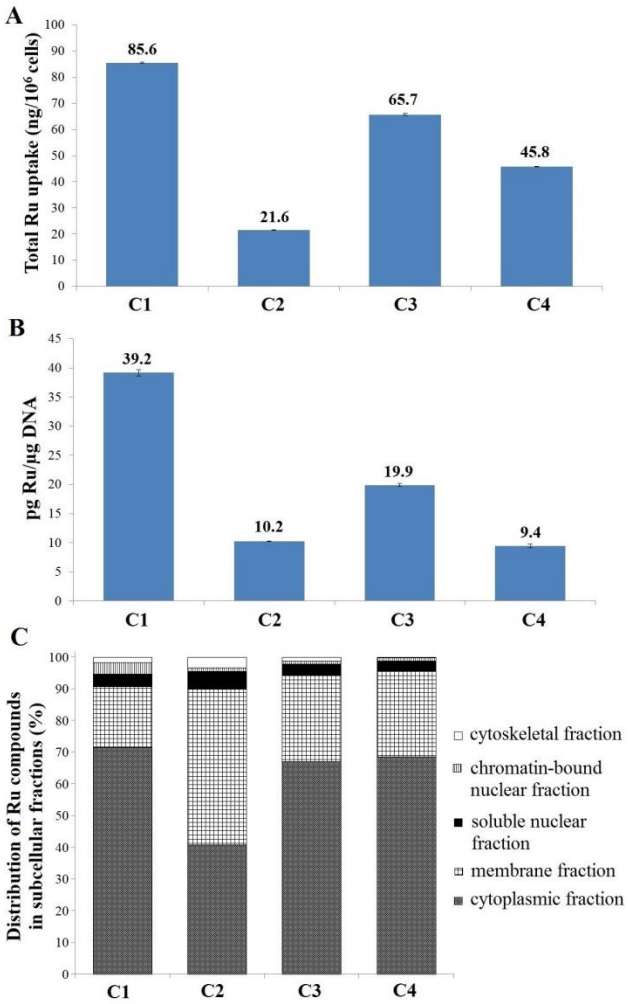

Figure 5. Bar graphs representing quantitative determination of the (**A**) total intracellular uptake (ng Ru/10^6 cells), (**B**) DNA binding (pg Ru/µg DNA), and (**C**) subcellular localization (percentage localizing in the cell fragments calculated on the basis that their sum was 100%) of **C1**-**C4** complexes after 200 µM treatment of HCC1937 cells for 24 h, measured by ICP-MS. Bar graphs represent the mean ± SD of at least two independent experiments.

4.7. Interaction with Plasmid DNA

The ability of ruthenium(II)-arene complexes and their starting binuclear complexes and ligands, to alter the tertiary structure of DNA, in a cell-free system, was determined by testing the electrophoretic mobility of pHOT-1 plasmid DNA. CDDP was tested as a reference compound. Small changes in the tertiary structure of DNA can easily be monitored on the plasmid DNA, since its superhelical nature mimics well certain forms of intracellular DNA, such as chromatin. The supercoiled form of DNA (Form I) experiences less resistance from

the gel, due to its compact nature and migrate faster, whereas open (nicked) circular form (Form II) moves slower through the gel. As shown in Figure 6, pHOT-1 plasmid consisted mainly of Form I and Form II. Addition of CDDP to the plasmid resulted in a gradual disappearance of two distinct bands representing Form I and Form II, and in the consequent formation of one smeared band. CDDP caused a concentration-dependent decrease in the rate of migration of Form I, and at the same time accelerated mobility of Form II. At 25 μM, CDDP caused a significant decrease in the rate of migration of Form I, due to probable relaxation (unwinding) of the supercoiled DNA. At higher concentrations (50 μM and 100 μM), CDDP caused coalescence of Form I and Form II bands. This observation indicated local untwisting at the sites of CDDP-DNA adducts and was in accordance with the previous literature data [99,100].

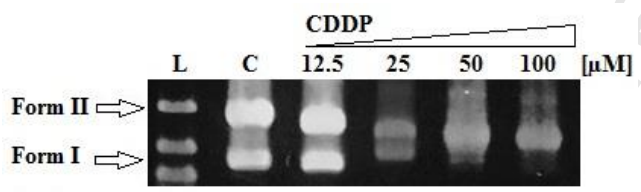

Figure 6. Agarose gel electrophoretic analysis of pHOT-1 plasmid DNA (300 ng) incubated with 12.5 μM, 25 μM, 50 μM, and 100 μM CDDP, for 24 h, in a 5 mM Tris-HCl/50 mM NaCl buffer, pH 7.2, at 37°C. L: DNA ladder; C: pHOT-1 plasmid DNA (300 ng).

Incubation of pHOT-1 plasmid DNA with ligands **L1** and **L2**, at concentrations corresponding to 200 μM and 400 μM, did not induce any significant alterations in the tertiary structure of plasmid DNA that could be visualized (Figure 7A). Of interest, two investigated ruthenium(II)-arenes, **C5** and **C6**, altered electrophoretic mobility of pHOT-1 plasmid DNA (Figure 7B). **C5** displayed the capability to interact with plasmid DNA, and 200 μM treatment induced untwisting of supercoiled Form I, and appearance of the smeared band. This effect can be explained by the capacity of complex to form adducts with plasmid DNA, that in turn, induce unwinding of the negatively supercoiled helix, and reduction in the number of negative supercoils, leading to slower mobility of plasmid bands. Interestingly, **C5**

(at 400 µM) and **C6** (at 200 µM), caused disappearance of Form I and Form II bands, and formation of one band, whose mobility exceeded that of the supercoiled Form I. This result indicated enhanced coiling, and formation of more compact DNA structure upon **C5** or **C6** binding, implicating the role of Ru(II) metal center in DNA binding and damage.

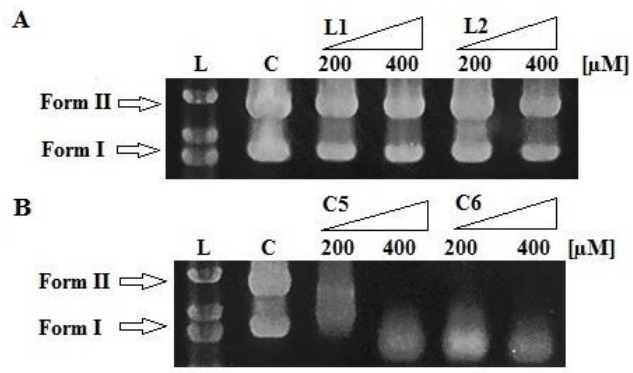

Figure 7. Agarose gel electrophoretic analysis of pHOT-1 plasmid DNA (300 ng) incubated with 200 µM and 400 µM (**A**) ligands (**L1**, **L2**) and (**B**) ruthenium(II)-arenes (**C5**, **C6**), for 24 h, in a 5 mM Tris-HCl/50 mM NaCl buffer, pH 7.2, at 37°C. L: DNA ladder; C: pHOT-1 plasmid DNA (300 ng).

Although 200 µM treatment with **C1**-**C4** did not alter the electrophoretic mobility of pHOT-1 plasmid DNA, increasing concentration to 400 µM caused various changes in the mobility of plasmid DNA (Figure 8). **C1** showed the capability to interact with plasmid DNA, as seen from the appearance of low intensity smeared band, in the line between Form I and Form II. **C2** and **C3** induced relaxation and unwinding of the supercoiled Form I, and mobility shift,to some extent. In contrast, **C4** caused the appearance of a low-intensity band with higher mobility than the respective control plasmid DNA, indicating profound coiling and DNA condensation, as observed also with its parental ruthenium(II)-*p*-cymene, **C6**. The degree of super helicity of the plasmid DNA has been altered to ascertain degree by all tested complexes, which correlates to the previous reports for ruthenium(II)-arenes [69,101]. Since unwinding of the double strand of DNA helix can be caused by the formation of monofunctional or intercalating adducts [102], our findings suggest again that tested ruthenium complexes manifest their activity, at least partly through interaction with DNA. To

further investigate possible DNA binding preferences of four complexes, gel electrophoretic analysis of treated pHOT-1 plasmid DNA was performed, in the presence of the minor groove binding agent, 4′,6-diamidino-2-phenylindole(DAPI), and major groove binding agent, methyl green (MG) [103]. The supercoiled pHOT-1 plasmid was treated separately with DAPI and MG, prior to the addition of **C1**-**C4**. When applying 400 μM of complexes, there were no significant alterations in the mobility pattern of plasmid forms, suggesting that **C1**-**C4** complexes do not compete with DAPI or MG for DNA binding sites, and therefore do not act either as minor or as major groove binders (Figure 9A, B). Treatment of DAPI- or MG-bound plasmid DNA with **C1**-**C4** displayed lower intensity bands than treatment with complexes only. It is well known that GelRed, as a standard gel staining dye, acts by intercalation and groove binding, preferably to the minor groove of DNA [104]. Disappearance of the plasmid DNA bands implies significant saturation of the GelRed binding sites and strong DNA intercalating potential of investigated ruthenium complexes (especially seen for **C1** and **C4**), so staining of the gel for DNA visualization appeared as less efficient.

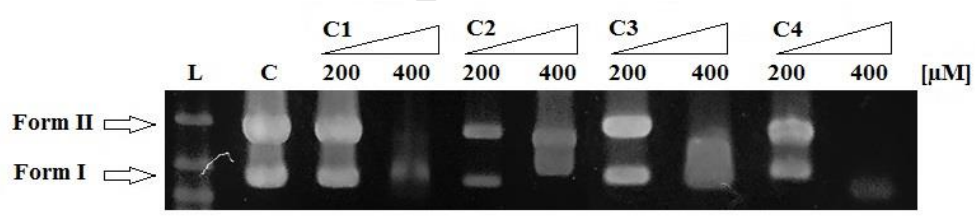

Figure 8. Agarose gel electrophoretic analysis of pHOT-1 plasmid DNA (300 ng) incubated with 200 μM and 400 μM ruthenium complexes (**C1**-**C4**), for 24 h, in a 5 mM Tris-HCl/50 mM NaCl buffer, pH 7.2, at 37°C. L: DNA ladder; C: pHOT-1 plasmid DNA (300 ng).

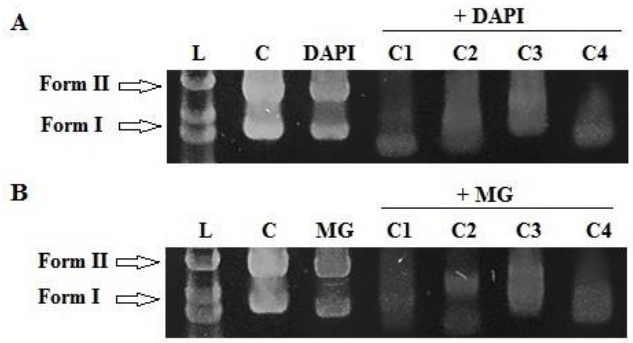

Figure 9. Agarose gel electrophoretic analysis of pHOT-1 plasmid DNA (300 ng) incubated with 400 µM ruthenium complexes (**C1**-**C4**), in the presence of (**A**) 100 µM DAPI, or (**B**) 100 µM MG (methyl green), for 24 h, in a 5 mM Tris-HCl/50 mM NaCl buffer, pH 7.2, at 37°C. L: DNA ladder; C: pHOT-1 plasmid DNA (300 ng).

5. Conclusions

In the present study, four new ruthenium(II)-arene complexes, **C1**-**C4**, carrying derivatives of 3-aminobenzamide, with anticipated multifunctional potential, were synthesized and tested for their anticancer activity *in vitro*. Complexes exhibited efficiency in inhibiting PARP-1 activity, at micromolar concentrations, in the following order: **C2**>**C4**>3-AB>**C1**>**C3**. Complexes bearing η^6-*p*-cymene moiety (**C2** and **C4**), demonstrated better PARP-1 inhibition than their starting complex **C6** and the benchmark PARP inhibitor 3-AB, suggesting that the ability of **C2** and **C4** to impair PARP-1 action may derive perhaps through interaction with the catalytic domain or zinc fingers of PARP-1 enzyme. Capability of precursor ruthenium(II)-*p*-cymene binuclear complex (**C6**) to inhibit PARP-1 indicates noteworthy affinity of this part of complex (and probably especially a metal center) alone to interfere with PARP-1 activity.

Investigated **C1**-**C4** complexes displayed growth inhibitory effects toward breast cancer cells, *BRCA1*-mutant (HCC1937), *BRCA1*-wild-type triple-negative (MDA-MB-231, MDA-MB-453), and hormone-responsive (MCF-7, MDA-MB-361), in the micromolar range of concentrations: 146.9-580.5 µM. Interestingly, three cell lines, HCC1937, MDA-MB-231

andMCF-7, displayed approximately 2-fold higher sensitivity to the action of complexes than MDA-MB-453 and MDA-MB-361 cells. **C1**, ([(η^6-toluene)Ru(**L1)**Cl]PF_6), exhibited the highest antiproliferative potential, with similar IC_{50} values across these cell lines. Structure-activity comparison revealed that bidentately coordinated ligands in ruthenium(II)-arene complexes potentiated biological action, as **C1** and **C2** exhibited higher activity than monodentately bound **C3** and **C4**. Further investigation of the mechanism of action of **C1**-**C4** in HCC1937 cells disclosed markedly relation between growth inhibitory potential of complexes and their cellular uptake. Results of the ICP-MS analysis revealed that **C1**-**C4** entered the HCC1937 cells following 24 h incubation, with efficiency (ng of Ru/10^6 treated cells) decreasing in order: **C1**>**C3**>**C4**>**C2**. Complexes **C1**, **C3** and **C4** mostly accumulated in the cytoplasm of HCC1937 cells (approximately 70%), allowing them to interact with various intracellular molecules and manifest their complex mechanism of action.

C1 displayed notable nuclear-targeting properties, as it was found evidently in the chromatin-bound nuclear fraction, showed the highest DNA binding affinity (39.2±0.6 pg of Ru per μg of DNA), and ability to interfere with the DNA replication (arrest of the cell cycle in the S phase). Furthermore, ICP-MS analysis in HCC1937 cells, and electrophoretic mobility study in a cell-free system, by using the pHOT-1 plasmid DNA, showed affinity of **C1** to bind DNA, and form DNA adducts. *In vitro* PARP-1 test revealed its potential for PARP-1 inhibition. Based on these results, we can conclude that **C1** demonstrated the potential to obstruct structural and functional properties of DNA (DNA replication), either through binding to DNA or interfering with PARP-1 activity, or by the combination of both. Additionally, **C1**-**C4** complexes may have other cellular targets that were not revealed in this study but could be anticipated from a remarkable amount of complexes found in the membrane and cytoplasmic fraction of cells. Complex **C2** showed the highest accumulation in the membrane fraction, and also selectivity for highly invasive MDA-MB-231 cells, thus may present a candidate for further investigation of antimetastatic potential.

Despite the low PARP-1 inhibitory potential of deriving benzamide-based ligands, our results pointed out that the ruthenium(II)-arene complexes **C1**, **C2** and **C4** exhibited enhanced ability to compromise PARP-1 enzymatic action. In recent years, it has become clear that many of the available PARP-1 inhibitors have polypharmacology profile, and may act at distant unrelated targets. Taken together, these results support the hypothesis of the multi-targeting affinity of ruthenium as a single agent, and justify the strategy based on the rational design of hybrid molecules, with metals coordinated to the bioactive ligand. This strategy may help in obtaining a new category of more potent anticancer drug candidates, with a broader spectrum of pharmacological activities in tumors harbouring *BRCA1* mutations.

Abbreviations

NAMI-A - Imidazolium-*trans*-[tetrachloro(dimethylsulfoxide)imidazoleruthenium(III)]

KP1339 - Sodium-*trans*-[tetrachlorobis(1H-indazole)ruthenium(III)]

RAPTA-C - (II)-dichloro(1,3,5-triaza-7-phosphaadamantane)(η^6-*p*-cymene)

RAED-C - Ruthenium(II)chloro(η^6-*p*-cymene)ethylenediamine-hexafluorophosphate

RAPTA-T - Ruthenium(II)-dichloro(1,3,5-triaza-7-phosphaadamantane)(η^6-toluene)

PARP - Poly(ADP-ribose) polymerase

ADP - Adenosine diphosphate

BER - Base excision repair

SSBs - Single-strand breaks

β-NAD^+ - Beta nicotinamide adenine dinucleotide

PAR - Poly(ADP-ribose)

PARPi - Poly(ADP-ribose) polymerase inhibitor

3-AB - 3-aminobenzamide

BRCA - Breast cancer susceptibility gene

DSBs - Double-strand breaks

HR - Homologous recombination

U.S. FDA - United States Food and Drug Administration

DMSO - Dimethyl sulfoxide

MTT - 3-(4.5-dimethylthiazol-2-yl)-2.5-diphenyltetrazolium bromide dye

CDDP - *cis*-diamminedichloroplatinum(II), cisplatin

PTEN - Phosphatase and tensin homolog gene

ICP-MS - Inductively coupled plasma mass spectrometry

DAPI - 4′,6-diamidino-2-phenylindole

MG - Methyl green

DMEM - Dulbecco's modified Eagle's medium

RPMI - Roswell Park Memorial Institute 1640nutrient medium

FCS - Fetal calf serum

HEPES - 4-(2-hydroxyethyl)piperazine-1-ethanesulfonic acid

SDS - Sodium dodecyl sulfate

SI - Selectivity index

PBS - Phosphate-buffered saline

PI - Propidium iodide

RNaseA - Ribonuclease A

FACS - Fluorescence-activated cell sorting

Strep-HRP - Streptavidin-horseradish peroxidase

TBE - Tris-borate-EDTA buffer

Acknowledgements

Ministry of Education, Science and Technological Development of the Republic of Serbia, Grant numbers III 41026 and 172035.

Declaration of competing interest

The authors declare that they have no known competing financial interests or personal relationships that could have appeared to influence the work reported in this paper

References:

[1] D. D. Von Hoff, R. Schilsky, C. M. Reichert, R. L. Reddick, M. Rozencweig, R. C. Young, F. M. Muggia, Toxic effects of cis-dichlorodiammineplatinum(II) in man, Cancer Treat. Rep. 63 (1979) 1527-1531.

[2] L. Astolfi, S. Ghiselli, V. Guaran, M. Chicca, E. Simoni, E. Olivetto, G. Lelli, A. Martini,Correlation of adverse effects of cisplatin administration in patients affected by solid tumours: a retrospective evaluation, Oncol. Rep. 29(2013) 1285-1292.doi: 10.3892/or.2013.2279

[3] R. Oun, Y. E. Moussa, N. J. Wheate,The side effects of platinum-based chemotherapy drugs: a review for chemists, Dalton Trans. 47 (2018) 6645-6653. doi: 10.1039/c8dt00838h

[4] P. V. Simpson, N. M. Desai, I. Casari, M. Massi, M. Falasca, Metal-based antitumor compounds: beyond cisplatin, Future Med. Chem. 11 (2019) 119-135.doi: 10.4155/fmc-2018-0248

[5] G. Gasser, N. Metzler-Nolte, The potential of organometallic complexes in medicinal chemistry, Curr. Opin. Chem. Biol. 16 (2012) 84-91.doi: 10.1016/j.cbpa.2012.01.013

[6] G. Sava, S. Pacor, G. Mestroni, E. Alessio, Na[trans-RuCl4(DMSO)Im], a metal complex of ruthenium with antimetastatic properties, Clin. Exp. Metastasis 10 (1992) 273-280.https://doi.org/10.1007/BF00133563

[7] M. R. Berger, F. T. Garzon, B. K. Keppler, D. Schmahl,Efficacy of new ruthenium complexes against chemically induced autochthonous colorectal carcinoma in rats, Anticancer Res. 9 (1989) 761-765.

[8] R. Trondl, P. Heffeter, C. R. Kowol, M. A. Jakupec, W. Bergerb, B. K. Keppler, NKP-1339, the first ruthenium-based anticancer drug on the edge to clinical application, Chem. Sci. 5 (2014) 2925. https://doi.org/10.1039/C3SC53243G

[9] N. R. Dickson , S. F. Jones , H. A. Burris , R. K. Ramanathan , G. J. Weiss , J. R. Infante, J. C. Bendell , W. McCulloch , D. D. Von Hoff, A phase I dose-escalation study of NKP-1339 in patients with advanced solid tumors refractory to treatment, J. Clin. Oncol. 29 (2011) 2607-2607. DOI: 10.1200/jco.2011.29.15_suppl.2607

[10] H. A. Burris, S. Bakewell, J. C. Bendell, J. Infante, S. F. Jones, D. R. Spigel, G. J. Weiss, R. K. Ramanathan, A. Ogden, D. Von Hoff, Safety and activity of IT-139, a ruthenium-based compound, in patients with advanced solid tumours: a first-in-human, open-label, dose-escalation phase I study with expansion cohort, ESMO Open 1 (2016) e000154.doi: 10.1136/esmoopen-2016-000154

[11] J. M. Rademaker-Lakhai, D. van den Bongard, D. Pluim, J. H. Beijnen, J. H. Schellens,A Phase I and pharmacological study with imidazolium-trans-DMSO-imidazole-tetrachlororuthenate, a novel ruthenium anticancer agent, Clin. Cancer Res. 10 (2004) 3717-3727.DOI:10.1158/1078-0432.CCR-03-0746

[12] S. Leijen, S. A. Burgers, P. Baas, D. Pluim, M. Tibben, E. van Werkhoven, E. Alessio, G. Sava, J. H. Beijnen, J. H. Schellens, Phase I/II study with ruthenium compound NAMI-A and gemcitabine in patients with non-small cell lung cancer after first line therapy, Invest. New Drugs 33 (2015) 201-214.doi: 10.1007/s10637-014-0179-1

[13] E. Alessio, L. Messori,NAMI-A and KP1019/1339, Two Iconic Ruthenium Anticancer Drug Candidates Face-to-Face: A Case Story in Medicinal Inorganic Chemistry, Molecules 24 (2019).doi:10.3390/molecules24101995

[14] B. S. Murray, M. V. Babak, C. G. Hartinger, P. J. Dyson, The development of RAPTA compounds for the treatment of tumors, Coordin. Chem. Rev. 306 (2016) 86-114. doi:10.1016/j.ccr.2015.06.014

[15] G. Suss-Fink,Areneruthenium complexes as anticancer agents, Dalton Trans. 39 (2010) 1673-1688.https://doi.org/10.1039/B916860P

[16] Y. K. Yan, M. Melchart, A. Habtemariam, P. J. Sadler,Organometallic chemistry, biology and medicine: ruthenium arene anticancer complexes, Chem. Commun. (Camb) (2005) 4764-4776.https://doi.org/10.1039/B508531B

[17] P. J. Dyson, Systematic Design of a Targeted Organometallic Antitumour Drug in Pre-clinical Development, Chimia 61 (2007) 698-703.https://doi.org/10.2533/chimia.2007.698

[18] C. Scolaro, A. Bergamo, L. Brescacin, R. Delfino, M. Cocchietto, G. Laurenczy, T. J. Geldbach, G. Sava, P. J. Dyson,In Vitro and in Vivo Evaluation of Ruthenium(II)−Arene PTA Complexes, J. Med. Chem. 48 (2005) 4161-4171.https://doi.org/10.1021/jm050015d

[19] A. Bergamo, A. Masi, P. J. Dyson, G. Sava,Modulation of the metastatic progression of breast cancer with an organometallic ruthenium compound, Int. J. Oncol. 33(2008) 1281-1289.

[20] B. Biersack, Anticancer Activity and Modes of Action of (arene) ruthenium(II) Complexes Coordinated to C-, N-, and O-ligands, Mini Rev. Med. Chem. 16 (2016) 804-814.

[21] N. Gligorijevic, S. Arandelovic, L. Filipovic, K. Jakovljevic, R. Jankovic, S. Grguric-Sipka, I. Ivanovic, S. Radulovic, Z. Tesic,Picolinate ruthenium(II)-arene complex with in vitro antiproliferative and antimetastatic properties: comparison to a series of ruthenium(II)-arene complexes with similar structure, J. Inorg. Biochem. 108 (2012) 53-61.doi: 10.1016/j.jinorgbio.2011.12.002

[22] S. Nikolić, D. M. Opsenica, V. Filipović, B. Dojčinović, S. Aranđelović, S. Radulović, S. Grgurić-Šipka, Strong in Vitro Cytotoxic Potential of New Ruthenium–Cymene Complexes, Organometallics 34 (2015) 3464-3473.https://doi.org/10.1021/acs.organomet.5b00041

[23] K. K. Jovanovic, M. Tanic, I. Ivanovic, N. Gligorijevic, B. P. Dojcinovic, S. Radulovic, Cell cycle, apoptosis, cellular uptake and whole-transcriptome microarray gene expression analysis of HeLa cells treated with a ruthenium(II)-arene complex with an

isoquinoline-3-carboxylic acid ligandJ. Inorg. Biochem. 163 (2016) 362-373.doi: 10.1016/j.jinorgbio.2016.04.011

[24] S. Nikolic, L. Rangasamy, N. Gligorijevic, S. Arandelovic, S. Radulovic, G. Gasser, S. Grguric-Sipka, Synthesis, characterization and biological evaluation of novel Ru(II)-arene complexes containing intercalating ligands, J. Inorg. Biochem.160 (2016) 156-165.https://doi.org/10.1016/j.jinorgbio.2016.01.005

[25] G. Golbaghi, M. M. Haghdoost, D. Yancu, Y. L. L. Santos, N. Doucet, S. A. Patten, J. T. Sanderson, A. Castonguay,Organoruthenium(II) Complexes Bearing an Aromatase Inhibitor: Synthesis, Characterization, in Vitro Biological Activity and in Vivo Toxicity in Zebrafish Embryos, Organometallics 38 (2019) 702-711.doi: 10.1021/acs.organomet.8b00897

[26] M. K. Mohamed Subarkhan, L. Ren, B. Xie, C. Chen, Y. Wang, H. Wang,Novel tetranuclear ruthenium(II) arene complexes showing potent cytotoxic and antimetastatic activity as well as low toxicity in vivo, Eur. J. Med. Chem. 179 (2019) 246-256.doi: 10.1016/j.ejmech.2019.06.061

[27] V. Brabec, O. Novakova, DNA binding mode of ruthenium complexes and relationship to tumor cell toxicity, Drug Resist. Updat. 9 (2006) 111-122.https://doi.org/10.1016/j.drup.2006.05.002

[28] B. J. Reedijk,Metal-ligand exchange kinetics in platinum and ruthenium complexes, Platin. Met. Rev. 52 (2008) 2-11. doi: 10.1595/147106708X255987

[29] G. Sava, A. Bergamo, P. J. Dyson, Metal-based antitumour drugs in the post-genomic era: what comes next?, Dalton Trans. 40 (2011) 9069-9075. doi: 10.1039/c1dt10522a

[30] M. Raudenska, J. Balvan, M. Fojtu, J. Gumulec, M. Masarik, Unexpected therapeutic effects of cisplatin, Metallomics 11 (2019) 1182-1199.https://doi.org/10.1039/C9MT00049F

[31] G. Palermo, A. Magistrato, T. Riedel, T. von Erlach, C. A. Davey, P. J. Dyson, U. Rothlisberger, Fighting Cancer with Transition Metal Complexes: From Naked DNA to

Protein and Chromatin Targeting Strategies, ChemMedChem 11 (2016) 1199-1210.doi: 10.1002/cmdc.201500478

[32] R. G. Kenny, C. J. Marmion,Toward Multi-Targeted Platinum and Ruthenium Drugs—A New Paradigm in Cancer Drug Treatment Regimens?, Chem. Rev. 119 (2019) 1058-1137.https://doi.org/10.1021/acs.chemrev.8b00271

[33] G. Gasser, N. Metzler-Nolte, in Bioinorganic Medicinal Chemistry (Ed.: E. Allesio), Wiley, New York, 2011, pp. 351-382.

[34] K. J. Kilpin, P. J. Dyson, Enzyme inhibition by metal complexes: concepts, strategies and applications, Chem. Sci. 4 (2013) 1410-1419.doi: 10.1039/C3SC22349C

[35] Z. Yuan, S. Chen, Q. Sun, N. Wang, D. Li, S. Miao, C. Gao, Y. Chen, C. Tan, Y. Jiang, Olaparib hydroxamic acid derivatives as dual PARP and HDAC inhibitors for cancer therapy, Bioorg. Med. Chem. 25 (2017) 4100-4109.doi: 10.1016/j.bmc.2017.05.058

[36] A. Ohmoto, S. Yachida, Current status of poly(ADP-ribose) polymerase inhibitors and future directions, OncoTargets Ther. 10 (2017) 5195-5208.doi: 10.2147/OTT.S139336

[37] F. J. Bock, P. Chang, New directions in poly(ADP- ribose) polymerase biology, FEBS J. 283 (2016) 4017-4031. doi:10.1111/febs.13737

[38] J. S. Brown, B. O'Carrigan, S. P. Jackson, T. A. Yap, Targeting DNA Repair in Cancer: Beyond PARP Inhibitors, Cancer Discov. 7 (2017) 20-37.doi: 10.1158/2159-8290.CD-16-0860

[39] T. Zaremba, N. J. Curtin, PARP Inhibitor Development for Systemic Cancer Targeting, Anticancer Agents Med. Chem. 7(2007) 515-523.doi: 10.2174/187152007781668715

[40] L. Gatti, P. Perego,Orchestration of DSB repair: a novel BRCA2 connection, Cell Cycle 14 (2015) 2195-2196.doi: 10.1080/15384101.2015.1056614

[41] Z. Tao, P. Gao, H. W. Liu,Identification of the ADP-Ribosylation Sites in the PARP-1 Automodification Domain: Analysis and Implications, J. Am. Chem. Soc. 131 (2009) 14258-14260.https://doi.org/10.1021/ja906135d

[42] P. G. Jain, B. D. Patel, Medicinal chemistry approaches of poly ADP-Ribose polymerase 1 (PARP1) inhibitors as anticancer agents - A recent update, Eur. J. Med. Chem. 165 (2019) 198-215.https://doi.org/10.1016/j.ejmech.2019.01.024

[43] M. De Vos, V. Schreiber, F. Dantzer,The diverse roles and clinical relevance of PARPs in DNA damage repair: current state of the art, Biochem. Pharmacol. 84 (2012) 137-146.doi: 10.1016/j.bcp.2012.03.018

[44] A. T. A. Boraei, P. K. Singh, M. Sechi, S. Satta, Discovery of novel functionalized 1,2,4-triazoles as PARP-1 inhibitors in breast cancer: Design, synthesis and antitumor activity evaluation, Eur. J. Med. Chem. 182 (2019) 111621.doi: 10.1016/j.ejmech.2019.111621

[45] M. R. Purnell, W. J. Whish, Novel inhibitors of poly(ADP-ribose) synthetase, Biochem. J. 185 (1980) 775-777.doi: 10.1042/bj1850775

[46] D. Passeri, E. Camaioni, P. Liscio, P. Sabbatini, M. Ferri, A. Carotti, N. Giacche, R. Pellicciari, A. Gioiello, A. Macchiarulo, Concepts and Molecular Aspects in the Polypharmacology of PARP-1 Inhibitors, ChemMedChem 11 (2016) 1219-1226.doi: 10.1002/cmdc.201500391

[47] V. Cepeda, M. A. Fuertes, J. Castilla, C. Alonso, C. Quevedo, M. Soto, J. M. Perez, Poly(ADP-ribose) polymerase-1 (PARP-1) inhibitors in cancer chemotherapy, Recent Pat. Anticanc. 1 (2006) 39-53. doi : 10.2174/157489206775246430

[48] G. Kim, G. Ison, A. E. McKee, H. Zhang, S. Tang, T. Gwise, R. Sridhara, E. Lee, A. Tzou, R. Philip, H. J. Chiu, T. K. Ricks, T. Palmby, A. M. Russell, G. Ladouceur, E. Pfuma, H. Li, L. Zhao, Q. Liu, R. Venugopal, A. Ibrahim, R. Pazdur, FDA Approval Summary: Olaparib Monotherapy in Patients with Deleterious Germline BRCA-Mutated Advanced

Ovarian Cancer Treated with Three or More Lines of Chemotherapy, Clin. Cancer Res. 21 (2015) 4257-4261.doi: 10.1158/1078-0432.CCR-15-0887

[49] C. J. Lord, A. Ashworth, PARP inhibitors: Synthetic lethality in the clinic, Science 355 (2017) 1152-1158.DOI: 10.1126/science.aam7344

[50] S. E. Caulfield, C. C. Davis, K. F. Byers, Olaparib: A Novel Therapy for Metastatic Breast Cancer in Patients With a BRCA1/2 Mutation, J Adv Pract Oncol 10 (2019) 167-174.

[51] N. J. Curtin, C. Szabo,Therapeutic applications of PARP inhibitors: Anticancer therapy and beyond, Mol. Aspects Med. 34 (2013) 1217-1256.https://doi.org/10.1016/j.mam.2013.01.006

[52] H. Farmer, N. McCabe, C. J. Lord, A. N. Tutt, D. A. Johnson, T. B. Richardson, M. Santarosa, K. J. Dillon, I. Hickson, C. Knights, N. M. Martin, S. P. Jackson, G. C. Smith, A. Ashworth, Targeting the DNA repair defect in BRCA mutant cells as a therapeutic strategy, Nature 434 (2005) 917-921.https://doi.org/10.1038/nature03445

[53] H. E. Bryant, N. Schultz, H. D. Thomas, K. M. Parker, D. Flower, E. Lopez, S. Kyle, M. Meuth, N. J. Curtin, T. Helleday, Specific killing of BRCA2-deficient tumours with inhibitors of poly(ADP-ribose) polymerase, Nature 434 (2005) 913-917. doi: 10.1038/nature03443

[54] A. Ashworth, C. J. Lord, J. S. Reis-Filho, Genetic Interactions in Cancer Progression and Treatment, Cell 145 (2011) 30-38.https://doi.org/10.1016/j.cell.2011.03.020

[55] C. J. Lord, A. Ashworth, PARP inhibitors: Synthetic lethality in the clinic, Nat. Rev. Cancer 16 (2016) 110-120.DOI: 10.1126/science.aam7344

[56] N. McCabe, N. C. Turner, C. J. Lord, K. Kluzek, A. Bialkowska, S. Swift, S. Giavara, M. J. O'Connor, A. N. Tutt, M. Z. Zdzienicka, G. C. Smith, A. Ashworth,Deficiency in the repair of DNA damage by homologous recombination and sensitivity to poly(ADP-ribose) polymerase inhibition, Cancer Res. 66 (2006) 8109-8115. doi:10.1158/0008-5472.CAN-06-0140

[57] A. K. Byrum, A. Vindigni, N. Mosammaparast, Defining and Modulating 'BRCAness', Trends Cell Biol. 29 (2019) 740-751.doi: 10.1016/j.tcb.2019.06.005

[58] L. J. Barber, S. Sandhu, L. Chen, J. Campbell, I. Kozarewa, K. Fenwick, I. Assiotis, D. N. Rodrigues, J. S. Reis Filho, V. Moreno, J. Mateo, L. R. Molife, J. De Bono, S. Kaye, C. J. Lord, A. Ashworth,Secondary mutations in BRCA2 associated with clinical resistance to a PARP inhibitor,Secondary mutations in BRCA2 associated with clinical resistance to a PARP inhibitor, J. Pathol. 229 (2013) 422-429.doi: 10.1002/path.4140.

[59] A. Drean, C. J. Lord, A. Ashworth, PARP inhibitor combination therapy, Crit. Rev. Oncol. Hematol. 108 (2016) 73-85.doi: 10.1016/j.critrevonc.2016.10.010

[60] S. P. Basourakos, L. Li, A. M. Aparicio, P. G. Corn, J. Kim, T. C. Thompson, Combination Platinum-based and DNA Damage Response-targeting Cancer Therapy: Evolution and Future Directions, Curr. Med. Chem. 24 (2017) 1586-1606.doi: 10.2174/0929867323666161214114948

[61] E. R. Guggenheim, D. Xu, C. X. Zhang, P. V. Chang, S. J. Lippard, Photoaffinity isolation and identification of proteins in cancer cell extracts that bind to platinum-modified DNA, ChemBioChem 10 (2009) 141-157. doi: 10.1002/cbic.200800471

[62] G. Zhu, P. Chang, S. J. Lippard, Recognition of Platinum−DNA Damage by Poly(ADP-ribose) Polymerase-1, Biochemistry 49 (2010) 6177-6183.https://doi.org/10.1021/bi100775t

[63] E. Goodfellow, Z. Senhaji Mouhri, C. Williams, B. J. Jean-Claude,Design, synthesis and biological activity of novel molecules designed to target PARP and DNA, Bioorg. Med. Chem. Lett. 27 (2017) 688-694.https://doi.org/10.1016/j.bmcl.2016.09.054

[64] G. Golbaghi, A. Castonguay, Rationally Designed Ruthenium Complexes for Breast Cancer Therapy, Molecules 25(2) (2020) 265-290. https://doi.org/10.3390/molecules25020265

[65] Z. Wang, H. Qian, S. M. Yiu, J. Sun, G. Zhu,Multi-targeted organometallic ruthenium(II)–arene anticancer complexes bearing inhibitors of poly(ADP-ribose) polymerase-1: A strategy to improve cytotoxicity, J. Inorg. Biochem. 131 (2014) 47-55.https://doi.org/10.1016/j.jinorgbio.2013.10.017

[66] F. Mendes, M. Groessl, A. A. Nazarov, Y. O. Tsybin, G. Sava, I. Santos, P. J. Dyson, A. Casini,Metal-Based Inhibition of Poly(ADP-ribose) Polymerase − The Guardian Angel of DNA, J. Med. Chem. 54 (2011) 2196-2206. https://doi.org/10.1021/jm2000135

[67] S. B. Jensen, S. J. Rodger, M. D. Spicer, Facile preparation of η6-p-cymene ruthenium diphosphine complexes. Crystal structure of [(η^6-*p*-cymene)Ru(dppf)Cl]PF_6, J. Organomet. Chem. 556 (1998) 151-158.https://doi.org/10.1016/S0022-328X(97)00776-6

[68] R. A. Zelonka, M. C. Baird, Benzene Complexes of Ruthenium(II), Can. J. Chem. 50 (1972) 3063-3072.https://doi.org/10.1139/v72-486

[69] A. Tadić, J. Poljarević, M. Krstić, M. Kajzerberger, S. Aranđelović, S. Radulović, C. Kakoulidou, A. N. Papadopoulos, G. Psomas, S. Grgurić-Šipka,Ruthenium–arene complexes with NSAIDs: synthesis, characterization and bioactivity, New J. Chem. 42 (2018) 3001-3019.https://doi.org/10.1039/C7NJ04416J

[70] R. Supino, in In Vitro Toxicity Testing Protocols, Vol. 43 (Eds.: S. O'Hare, C. K. Atterwill), Humana Press, New Jersey, 1995, pp. 137-149.

[71] M. G. Ormerod, in Flow Cytometry, a Practical Approach (Ed.: M. G. Ormerod), Oxford University Press, New York, 1994, pp. 119-125.

[72] M. Pavlovic, S. Nikolic, N. Gligorijevic, B. Dojcinovic, S. Arandelovic, S. Grguric-Sipka, S. Radulovic,New organoruthenium compounds with pyrido[2′,3′:5,6]pyrazino[2,3-f][1,10]phenanthroline: synthesis, characterization, cytotoxicity, and investigation of mechanism of action, J. Biol. Inorg. Chem. 24 (2019) 297-310.https://doi.org/10.1007/s00775-019-01647-4

[73] S. A. Miller, D. D. Dykes, H. F. Polesky,A simple and efficient non-organic procedure for the isolation of genomic DNA from blood, Nucleic Acids Res. 16 (1988) 1215-1215.doi: 10.1093/nar/17.20.8390

[74] Z. Kozomara, G. Supic, A. Krivokuca, Z. Magic, R. Dzodic, Z. Milovanovic, M. Brankovic-Magic, Promoter hypermethylation of p16, BRCA1 and RASSF1A genes in triple-negative breast cancer patients from Serbia, J. BUON 23 (2018) 684-691.

[75] I. Ott, C. Biot, C. G. Hartinger, in Inorganic Chemical Biology: Principles, Techniques and Applications (Ed.: G. Gasser), John Wiley & Sons Inc, New York, 2014, pp. 63-97.

[76] Y.-R. Lee, D.-S. Yu, Y.-C. Liang, K.-F. Huang, S.-J. Chou, T.-C. Chen, C.-C. Lee, C.-L. Chen, S.-H. Chiou, H.-S. Huang, New Approaches of PARP-1 Inhibitors in Human Lung Cancer Cells and Cancer Stem-Like Cells by Some Selected Anthraquinone-Derived Small Molecules, PLoS One 2013, 8, e56284-e56284.

[77] P. Y. Lee, J. Costumbrado, C.-Y. Hsu, Y. H. Kim, Agarose Gel Electrophoresis for the Separation of DNA Fragments, J. Vis. Exp. 2012, 3923.

[78] M. Patra, T. Joshi, V. Pierroz, K. Ingram, M. Kaiser, S. Ferrari, B. Spingler, J. Keiser, Gilles Gasser, DMSO-Mediated Ligand Dissociation: Renaissance for Biological Activity of N-Heterocyclic-[Ru(η^6-arene)Cl_2] Drug Candidates, Chem. Eur. J. 19 (2013) 14768 – 14772. DOI: 10.1002/chem.201303341

[79] L. Biancalana, A. Pratesi, F. Chiellini, S. Zacchini, T. Funaioli, C. Gabbiani, Fabio Marchetti, Ruthenium arene complexes withtriphenylphosphane ligands: cytotoxicity towardspancreatic cancer cells, interaction with modelproteins, and effect of ethacrynic acid substitution, NewJ.Chem. 41 (2017) 14574-14588. DOI: 10.1039/c7nj02300f

[80] W. J. Geary, The use of conductivity measurements in organic solvents for the characterisation of coordination compounds, Coordin. Chem. Rev. 7 (1971) 81-122. https://doi.org/10.1016/S0010-8545(00)80009-0

[81] S. J. Dougan, P. J. Sadler, The Design of Organometallic Ruthenium Arene Anticancer Agents, Chimia 61 (2007) 704-715. doi:10.2533/chimia.2007.704

[82] F. Wang, A. Habtemariam, E. P. L. van der Geer, R. Fernández, M. Melchart, R. J. Deeth, R. Aird, S. Guichard, F. P. A. Fabbiani, P. Lozano-Casal, I. D. H. Oswald, D. I. Jodrell, S. Parsons, P. J. Sadler, Controlling ligand substitution reactions of organometallic complexes: Tuning cancer cell cytotoxicity, PNAS 102 (2005) 18269-18274. doi.org/10.1073/pnas.0505798102.

[83] S. Grgurić-Šipka, I. Ivanović, G. Rakić, N. Todorović, N. Gligorijević, S. Radulović, V. B. Arion, B. K. Keppler, Ž. Lj. Tešić, Ruthenium(II)–arene complexes with functionalized pyridines: Synthesis, characterization and cytotoxic activity, Eur J Med Chem. 45 (2010) 1051-1058. doi: 10.1016/j.ejmech.2009.11.055

[84] N. J. Curtin, PARP inhibitors for cancer therapy, Expert Rev. Mol. Med. 7 (2005) 1-20.DOI: https://doi.org/10.1017/S146239940500904X

[85] P. A. Kenny, G. Y. Lee, C. A. Myers, R. M. Neve, J. R. Semeiks, P. T. Spellman, K. Lorenz, E. H. Lee, M. H. Barcellos-Hoff, O. W. Petersen, J. W. Gray, M. J. Bissell, HER2 signaling pathway activation and response of breast cancer cells to HER2-targeting agents is dependent strongly on the 3D microenvironment, Mol. Oncol. 1 (2007) 84-96.https://doi.org/10.1007/s10549-009-0502-2

[86] V. J. Bhute, Y. Ma, X. Bao, S. P. Palecek,The Poly (ADP-Ribose) Polymerase Inhibitor Veliparib and Radiation Cause Significant Cell Line Dependent Metabolic Changes in Breast Cancer Cells, Sci. Rep. 6 (2016) 36061.https://doi.org/10.1038/srep36061

[87] R. M. Neve, K. Chin, J. Fridlyand, J. Yeh, F. L. Baehner, T. Fevr, L. Clark, N. Bayani, J. P. Coppe, F. Tong, T. Speed, P. T. Spellman, S. DeVries, A. Lapuk, N. J. Wang, W. L. Kuo, J. L. Stilwell, D. Pinkel, D. G. Albertson, F. M. Waldman, F. McCormick, R. B. Dickson, M. D. Johnson, M. Lippman, S. Ethier, A. Gazdar, J. W. Gray,A collection of breast

cancer cell lines for the study of functionally distinct cancer subtypes, Cancer Cell 10 (2006) 515-527.https://doi.org/10.1016/j.ccr.2006.10.008

[88] G. E. Tomlinson, T. T. Chen, V. A. Stastny, A. K. Virmani, M. A. Spillman, V. Tonk, J. L. Blum, N. R. Schneider, Wistuba, II, J. W. Shay, J. D. Minna, A. F. Gazdar, BRCA2 Is Required for Ionizing Radiation-induced Assembly of Rad51 Complex in Vivo, Cancer Res. 58 (1998) 3237-3242.

[89] G. Sava, R. Gagliardi, A. Bergamo, E. Alessio, G. Mestroni, Treatment of metastases of solid mouse tumours by NAMI-A: comparison with cisplatin, cyclophosphamide and dacarbazine, Anticancer Res. 19 (1999) 969–972.

[90] A. Bergamo, M. Gerdol, M. Lucafò, C. Pelillo, M. Battaglia, A. Pallavicini, G. Sava, RNA-seq analysis of the whole transcriptome of MDA-MB-231 mammary carcinoma cells exposed to the antimetastatic drug NAMI-A, Metallomics 7 (2015) 1439-1450. doi.org/10.1039/C5MT00081E

[91] K. A. Menear, C. Adcock, R. Boulter, X. L. Cockcroft, L. Copsey, A. Cranston, K. J. Dillon, J. Drzewiecki, S. Garman, S. Gomez, H. Javaid, F. Kerrigan, C. Knights, A. Lau, V. M. Loh, Jr., I. T. Matthews, S. Moore, M. J. O'Connor, G. C. Smith, N. M. Martin, 4-[3-(4-Cyclopropanecarbonylpiperazine-1-carbonyl)-4-fluorobenzyl]-2H-phthalazin-1-one: A Novel Bioavailable Inhibitor of Poly(ADP-ribose) Polymerase-1, J. Med. Chem. 51 (2008) 6581-6591.https://doi.org/10.1021/jm8001263

[92] G. Peng, C. Chun-Jen Lin, W. Mo, H. Dai, Y. Y. Park, S. M. Kim, Y. Peng, Q. Mo, S. Siwko, R. Hu, J. S. Lee, B. Hennessy, S. Hanash, G. B. Mills, S. Y. Lin,Genome-wide transcriptome profiling of homologous recombination DNA repair, Nat. Commun. 5 (2014) 3361.https://doi.org/10.1038/ncomms4361

[93] L. H. Saal, S. K. Gruvberger-Saal, C. Persson, K. Lovgren, M. Jumppanen, J. Staaf, G. Jonsson, M. M. Pires, M. Maurer, K. Holm, S. Koujak, S. Subramaniyam, J. Vallon-Christersson, H. Olsson, T. Su, L. Memeo, T. Ludwig, S. P. Ethier, M. Krogh, M. Szabolcs,

V. V. Murty, J. Isola, H. Hibshoosh, R. Parsons, A. Borg,Recurrent gross mutations of the PTEN tumor suppressor gene in breast cancers with deficient DSB repair, Nat. Genet. 40 (2008) 102-107.https://doi.org/10.1038/ng.2007.39

[94] N. J. Curtin, Y. Drew, S. Sharma-Saha,Why BRCA mutations are not tumour-agnostic biomarkers for PARP inhibitor therapy, Nat. Rev. Clin. Oncol. 16 (2019) 725-726.https://doi.org/10.1038/s41571-019-0285-2

[95] K. M. Frizzell, W. L. Kraus, PARP inhibitors and the treatment of breast cancer: beyond BRCA1/2?, Breast Cancer Res. 11 (2009) 111.https://doi.org/10.1186/bcr2451

[96] M. Capula, C. Corno, B. El Hassouni, G. Li Petri, S. Arandelovic, A Brief Guide to Performing Pharmacological Studies In Vitro: Reflections from the EORTC-PAMM Course "Preclinical and Early-phase Clinical Pharmacology", Anticancer Res. 39 (2019) 3413-3418.doi: 10.21873/anticanres.13485

[97] T. Nhukeaw, P. Temboot, K. Hansongnern, A. Ratanaphan, Cellular responses of BRCA1-defective and triple-negative breast cancer cells and in vitro BRCA1 interactions induced by metallo-intercalator ruthenium(II) complexes containing chloro-substituted phenylazopyridine, BMC Cancer 14 (2014) 73.https://doi.org/10.1186/1471-2407-14-73

[98] T. Nhukeaw, K. Hongthong, P. J. Dyson, A. Ratanaphan, Cellular responses of BRCA1-defective HCC1937 breast cancer cells induced by the antimetastasis ruthenium(II) arene compound RAPTA-T, Apoptosis 24 (2019) 612-622.https://doi.org/10.1007/s10495-019-01544-w

[99] O. Tari, F. Gumus, L. Acik, B. Aydin, Synthesis, characterization and DNA binding studies of platinum(II) complexes with benzimidazole derivative ligands, Bioorg. Chem. 74 (2017) 272-283.https://doi.org/10.1016/j.bioorg.2017.08.015

[100] L. Corte-Real, F. Mendes, J. Coimbra, T. S. Morais, A. I. Tomaz, A. Valente, M. H. Garcia, I. Santos, M. Bicho, F. Marques, Anticancer activity of structurally related

ruthenium(II) cyclopentadienyl complexes, J. Biol. Inorg. Chem. 19 (2014) 853-867.https://doi.org/10.1007/s00775-014-1120-y

[101] S. Richter, S. Singh, D. Draca, A. Kate, A. Kumbhar, A. S. Kumbhar, D. Maksimovic-Ivanic, S. Mijatovic, P. Lonnecke, E. Hey-Hawkins,Antiproliferative activity of ruthenium(II) arene complexes with mono- and bidentate pyridine-based ligands, Dalton Trans. 45 (2016) 13114-13125.DOI: 10.1039/C6DT01782G

[102] C. G. Hartinger, S. Zorbas-Seifried, M. A. Jakupec, B. Kynast, H. Zorbas, B. K. Keppler, From bench to bedside--preclinical and early clinical development of the anticancer agent indazolium trans-[tetrachlorobis(1H-indazole)ruthenate(III)] (KP1019 or FFC14A), J. Inorg. Biochem. 100 (2006) 891-904. DOI: 10.1016/j.jinorgbio.2006.02.013)

[103] C. Icsel, V. T. Yilmaz, B. Cevatemre, M. Aygun, E. Ulukaya,Structures and anticancer activity of chlorido platinum(II) saccharinate complexes with mono- and dialkylphenylphosphines, J. Inorg. Biochem. 195 (2019) 39-50.https://doi.org/10.1016/j.jinorgbio.2019.03.008

[104] M. Anjomshoa, M. Torkzadeh-Mahani, Competitive DNA-Binding Studies between Metal Complexes and GelRed as a New and Safe Fluorescent DNA Dye, J. Fluoresc. 26 (2016) 1505-1510.https://doi.org/10.1007/s10895-016-1850-z

Graphical Abstract (figure):

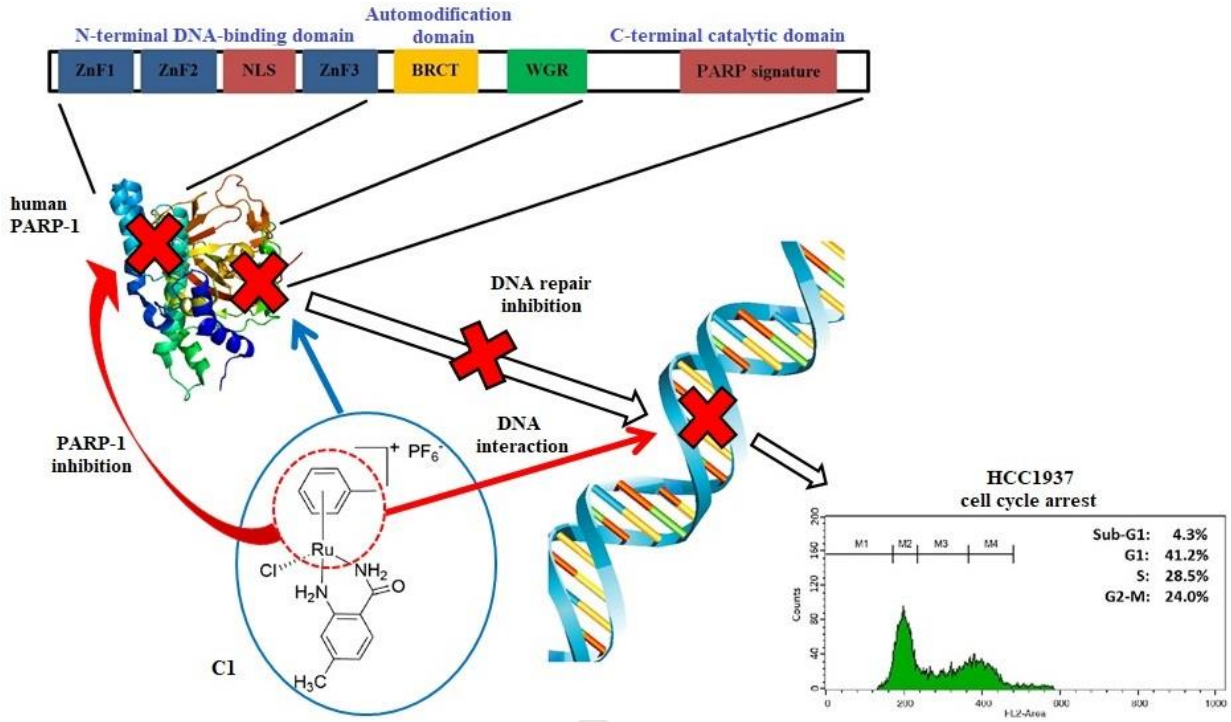

Graphical Abstract (synopsis): Designing the single molecule that simultaneously modulates multiple and specific targets, is paradigmin antitumor drug discovery. Here, we describe the synthesis, characterization, and *in vitro* antitumor activity of ruthenium(II)-arene complexes conjugated with 3-aminobenzamide derivatives, affecting PARP-1 enzymatic activity *in vitro* and interacting with DNA in human breast cancer cells.

Highlights

- Ru(II) arene complexes exhibit good efficiency in inhibiting PARP-1 activity
- Ru complexes exhibit good antiproliferative activity against breast cancer cells
- Ru(II) arene complexes display notable nuclear-targeting properties
- Ru(II) arene complexes interfere with the DNA replication